Understanding and control of the metallic state in epitaxial NdNiO3

Guo, Qikai

DOI:
10.33612/diss.180302851

Chapter 1

Introduction

As strongly-correlated electron systems, Rare-earth nickelates are reported to display a broad range of intriguing phenomena, such as a tunable metal-insulator transition, a negative charge-transfer insulating state, a Non-Fermi liquid and strange metal-like metallic state, and even a high-T_c superconductivity in its infinite-layer counterpart. At the same time, the hybridization of various concepts in a specific material also makes the understanding of the underlying physics a challenging task. In this chapter I describe the basic background that is needed to understand the concepts in this thesis. Those readers with a physics background are recommended to skip the first sections.

1.1 Electrical conduction

Electrical conduction describes the ability of charged particles to move through a given medium in response to an externally applied electric field. In a metal, the corresponding amount of charge carriers flowing through a unit area per unit time, named as current density $\boldsymbol{J}$, is determined by both the applied electrical field $\boldsymbol{E}$ and the conductivity σ of the given material, following Ohm's law:

$$\boldsymbol{J} = \sigma \boldsymbol{E} \tag{1.1}$$

According to their electrical conductivity, materials can be classified as conductors, semiconductors, or insulators. The conductivity of good conductors can be as high as 10^{10} Ω^{-1} m^{-1}, while that of insulators can be even lower than 10^{-22} Ω^{-1} m^{-1}. This gigantic difference over 32 orders of magnitude in conductivity is possibly the widest range found among the physical properties of solids [1]. For a long time, people were puzzled by the origin of this vast difference.

Herein, we begin our discussion with the early theories of conduction in metals. The first attempt to explain metallic conductivity (or its inverse, known as resistivity, ρ) was made by P. Drude in 1900 [2]. The most relevant charged particles in a solid are electrons in their atoms, moving in differently sized and shaped orbitals around the atoms nuclei. However, only those who can detach from the atoms un-

der E and move through the metal finally contribute to the conductivity. In Drude's model, he supposed these free electrons were all the valence electron (all the electrons in the highest energy, partially-filled electronic orbitals of the metal) and that they were fully independent of each other (non-interacting) behaving very much like the molecules in an ideal gas: moving randomly and undergoing elastic collisions with the ions in the crystal. Accordingly, their velocity was determined only by the temperature, following the equipartition theorem. Next to Ohm's law, Drude's model explained the Joule heating and the resistance of metals as transfer of kinetic energy between the electrons and the lattice as result of the collisions. Drude named the average time that the electrons travelled in between collisions as *relaxation time*, τ, and the average distance between collision events as *mean free path* $lambda$. The Drude conductivity can be calculated as:

$$\sigma = \frac{ne^2\tau}{m_e} \tag{1.2}$$

where m_e is the electron mass and n is the electron density.

However, Drude's model could not explain the conductivity in alloys (always less than that of the individual components [3]) or the observed linear temperature dependence of conductivities in metals, among other facts. With the development of quantum mechanics, some advances were presented by Sommerfeld and Bloch [4, 5]. Bloch postulated that electrons do not move randomly colliding with the ions but instead they meander through the lattice following a first attractive and then repulsive interaction, as they come in close proximity to the different ions in the periodic lattice. The meandering has, thus, the same periodicity as the crystal and the resistance of the material to the flow of current only originates from deviations of such periodicity, due to lattice vibrations or defects.

According to Pauli's exclusion principle [6] that limits the number of electrons that can exist with the same energy (in the same orbital) to 2, electrons in an atom fill up increasingly higher discrete energy states. In a solid made of N atoms, the energy levels of the 2N electrons of a particular orbital will slightly modify their energy, creating N energy levels so close to each other that it can be considered the electrons are part of an electronic *band*. Each band can host N times more electrons than the corresponding atomic level. The width of the bands is determined by the degree of overlap of the atomic orbitals, which is, in turn, determined by the crystal structure and the interatomic forces. As in the single atom, the electrons fill in the bands from the lowest to the highest energy and the probability of occupying a level with particular energy, ϵ, is given by the *Fermi-Dirac distribution* [7]:

$$f(\epsilon) = \frac{1}{e^{(\epsilon-\epsilon_\mathrm{F})/k_\mathrm{B}T}+1} \tag{1.3}$$

where k_B is the Boltzmann constant, ϵ is the energy of electrons, and ϵ_F is referred to as the Fermi energy, which characterizes the energy of the highest occupied state at T= 0 K. At this temperature, the Fermi Dirac distributions is, thus, a step function with probability of occupation being 1 for $\epsilon < \varepsilon_F$ and 0 for $\epsilon > \epsilon_F$. For increasing temperatures, the step function rounds off as the temperature increases, with an increasingly higher probability for electrons to occupy levels at $\epsilon > \epsilon_F$. Therefore, contrary to the hypothesis of Drude's model, only a small fraction of all valence electrons take part in conduction and their velocity is fixed by the ϵ_F and not determined by temperature.

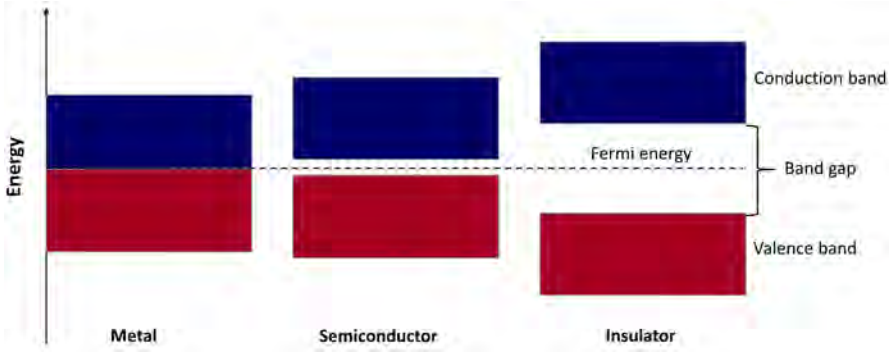

Figure 1.1: *Sketch of the electronic band diagrams showing the differences between metals, semiconductors, and insulators at 0 K. The valence electrons are in the red bands and the blue bands are the empty states from which the electrons can move through the solid under an electric field.*

In metals, the highest energy electronic band (valence band) is only partially filled (see Fig.1.1). In this case, the electrons under an applied electric field are able to increase their energy by occupying a vacant state in the same band and are free to move through the solid, giving rise to a high conductivity. On the contrary, in insulators, the valence band is completely filled and the next lowest energy available states are in a different band (named as the conduction band), therefore separated by a region of forbidden energies, known as the *energy gap* (ϵ_g), which is larger than the energy surplus provided by the electric field. Therefore, at absolute zero temperature the conduction band in insulators is empty, resulting in no conductivity. In this case, the E_F, which generally speaking, as indicated by Eq. 1.3, is the energy at which the probability of occupation is 0.5, is in the middle of the energy gap (half way between the highest occupied state and the lowest vacant state).

According to Eq. 1.3, the probability to find an electron with increased energy depends on the Fermi energy and the temperature. However, due to the large energy gap in insulators ($\epsilon_g > 3$ eV), it is very rare that an electron in the valence band can

be excited to the conduction band, resulting in a very small conductivity compared with metals. An intermediate situation between metals and insulators takes place in the case of *semiconductors*. In these materials, the valence band is only separated from the conduction band by a narrow energy gap ($\epsilon_g < 3$ eV) such that, at finite temperatures, the rounding off of the Fermi-Dirac distribution described above, allows electrons to get into the conduction band. These excited electrons contribute a non-zero conductivity in non-metals and to a strong temperature dependence. [1]

It is worth to note that, in many materials, the electrons are not the only charge carriers that can conduct electricity. The excitation of electrons to the conduction band leaves behind so-called *holes* in the valence band [8]. Each hole acts in an applied electric field as a particle with a positive charge $+e$. In some semiconductors, these positively charged holes even take a dominant role in determining the conductivity. The nature of the decisive charge carriers in a specific material can be determined from their performance in a magnetic field by measuring the *so-called Hall effect*, which will be discussed later.

Since its discovery, electronic band theory has represented a great success in explaining many electrical properties of conventional metals. However, the theory does not include electron-electron interactions and, thus, one needs to be careful to apply it to materials with transition metals (e.g Fe, Mn, Ni, etc.). The electrons in these systems interact strongly with each other, due to the nature of the electronic bands: these are composed by electrons in so-called d-orbitals, which can host many electrons with similar energy giving rise to "narrow" bands. These materials are referred to as strongly correlated electron systems or strongly correlated systems, displaying several phenomena that cannot be explained within the regime of Bloch band theory [9–11]. In the following sections, some of those directly related to this project are reviewed.

1.2 Metals

As mentioned above, the electrical resistance of metals mainly arises from the scattering of electrons with lattice vibrations (phonons), at large enough temperatures, as well as with defects and impurities, both of which decrease the electron mobility. However, scattering of electrons can also take place by interactions with other electrons and with other (quasi-)particles, such as magnons [13]. Following the nomenclature from Drude's model, the average distance for electrons travelling between two successive scattering events is named as *Mean-free-path* (ℓ). Correspondingly, the resistivity (ρ) of a three-dimensional system can be expressed in terms of ℓ as:

$$\rho = \frac{3\pi^2\hbar}{e^2 k_F^2 \ell} \tag{1.4}$$

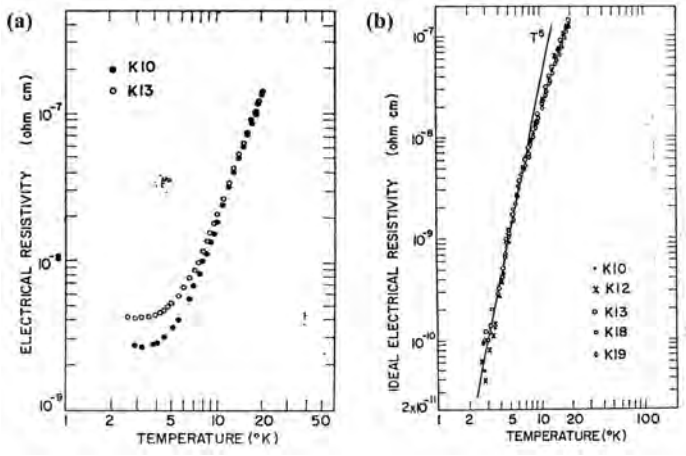

Figure 1.2: *(a) Electrical resistivity versus temperature in two potassium samples. (b) Temperature dependence of the ρ_i component of the resistivity (see Eq. 1.5) of various potassium samples. The T^5 fitting curve, expected for low-temperature electron-phonon scattering, is shown for comparison. (Reprinted with permission from Ref. [12])*

where the $\hbar$ is the reduced Planck constant and k_F is the Fermi wave vector, which represents the Fermi surface that separates the unoccupied states from the occupied states in momentum (reciprocal) k-space. The value of k_{F} is directly related to the electron density of the system ($k_F = (3\pi^2 n)^{1/3}$).

As well known, metals are characterized by their high electrical conductivity. However, it is usually not sufficient to identify a solid as metal only by the value of its conductivity in a specific temperature: on the one hand, the conductivity of some metals can be comparable with that of some (doped) semiconductors; on the other hand, the conductivity of solids shows a temperature dependence that can be very strong in the case of semiconductors. Normally, a reliable way to determine the nature of the conduction is performing measurements of resistivity as a function of temperature. A material can be regarded as a metal only if its resistivity exhibits $d\rho/dT > 0$; otherwise, it is an semiconductor. This guideline is built on the fact that the resistivity of metals mainly arise from the scattering of electrons with phonons, which increase in number with increasing temperature (as the vibration amplitude of the ions increases); while that of insulating (or semiconducting) behaviour is determined by the excitation of valence electrons across the band gap or the hopping of electrons from/to defect states (which will be discussed later). In this case, increasing temperature increases the number of charge carriers and, thus, the conductivity, decreasing the resistivity ($d\rho/dT < 0$). The temperature-dependence of resistivity ($\rho(T)$) for metals can be often described by the Matthiessen's rule [14]:

$$\rho(T) = \rho(0) + \rho_i(T) \tag{1.5}$$

where the $\rho(0)$ is the residual resistivity and represents the contribution of defects to the metallic resistivity. The approximate value of $\rho(0)$ in a specific metal can be evaluated either by fitting and extrapolation of the $\rho(T)$ curve or by measuring the resistivity near absolute zero. An example is given in Fig. 1.2 (a), the resistivity of the potassium samples approaches a constant value below 3 K. In this temperature regime, the scattering of electrons by other mechanisms becomes negligibly weak. Instead, most of the scattering events happen between electrons and defects, leaving a constant $\rho(0)$ value. The $\rho_i(T)$ is the resistivity of a metal after subtracting the contributions from defects. The study of the $\rho_i(T)$ dependence is significantly important in metal physics as it directly reflects the dominant scattering mechanisms that are relevant in a specific metal.

As mentioned above, in simple metals with wide electronic bands (e.g alkali metals), the electrons can be regarded as non-interacting Fermions (particles that follow Pauli's exclusion principle), and these metals are named as Fermi gases. In this case, the $\rho_i(T)$ is mainly determined by the scattering between electrons and lattice vibrations (phonons). Moreover, since higher temperatures induce larger amplitude of the vibrations, the strength of electron-phonon interactions increases correspondingly and then leads to a positive temperature dependence of $\rho_i(T)$, which can be approximated by the *Bloch-Gruneisen* Formula:

$$\rho_i(T) = \alpha_{ep}(\frac{T}{\theta_D})^n \int_0^{\theta_D/T} \frac{x^n}{(e^x - 1)(1 - e^{-x})} dx \tag{1.6}$$

where α_{ep} is a constant and θ_D is the Debye temperature that can be expressed as $\theta_D = \omega_D \hbar / K_B$, where ω_D is the ionic vibration frequency, which in turn is determined by the strength of the atomic bonding and the mass of the ions.

The total resistivity of a simple metal can be calculated by replacing the ρ_i in Eq. 1.5 with Eq. 1.6. The Bloch-Gruneisen formula predicts the scattering of electrons by phonons and gives rise to a T-linear dependence of resistivity ($\rho(T) \propto AT$) at high temperature ($T \gg \theta_D$); while in the low temperature regime, a Bloch $\rho(T) \propto T^5$ law (with n=5 in Eq. 1.6) caused by peculiarities of small angle scattering at very low temperature is obeyed. An example is given in Fig. 1.2 (b), in which a T^5 dependence is followed in various potassium samples below 7 K [12].

1.2.1 Fermi liquids

Because of the effect of *Coulomb interactions* between electrons becoming significantly important or even dominant in correlated oxides, especially at low-T, in these sys-

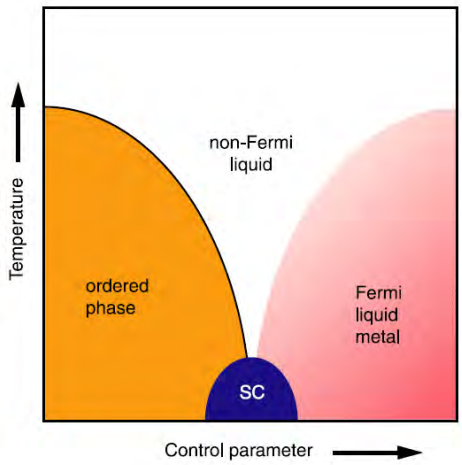

Figure 1.3: *Conventional phase diagram of a quantum critical point induced by a control parameter, which can be pressure, magnetic field, carrier doping, etc. Next to the Fermi liquid-like metallic phase (pink region), there is an ordered state (marked with orange); while the non-Fermi-liquid behaviour (white region) can only be achieved above the quantum critical point. The blue region at the bottom indicate a a superconducting dome (SC), which is partially overlapping with the quantum critical region. (Reprinted with permission from Ref. [15])*

tems, the Bloch-Gruneisen formula built on the dominant electron-phonon scattering meets with problems. To address this, in 1956 Landau introduced the concept of "Fermi liquid" in his series of works to describe the transport properties of systems of interacting fermions (electrons or holes) [16, 17]. With great insight, he argued there exists a one-to-one correspondence between states of interacting Fermi systems and those in free- electron systems (Fermi gases) if one substitutes the non-interacting fermions in the Fermi gas with *so-called* "fermion quasiparticles". These fermion quasiparticles have similar equilibrium properties than the free-electrons while displaying different wavefunctions and energies [18]. Hence, quantities such as specific heat and spin-susceptibility, which only arise from a well defined Fermi surface, shows the same temperature dependence in an interacting system as in the Fermi gas; while the dependence of resistivity with temperature is usually different in the two systems.

At absolute zero, the scattering rate of these fermion quasiparticles is proportional to their quadratic energy (ϵ^2) following [18, 19]:

$$\frac{1}{\tau_{ee}} \propto \frac{\pi}{\hbar}|V|^2 g_F^2 \epsilon^2 \tag{1.7}$$

where τ_{ee} is the lifetime (relaxation time) of the quasiparticles near the Fermi surface, g_F is the density of states at the Fermi surface, and $|V|$ is a model-dependent interaction potential. At finite temperature, the environment temperature sets a linear scale to the quasiparticle energy ($\epsilon \propto k_B T$) so that the resistivity, which is directly proportional to the scattering rate ($1/\tau_{ee}$), follows a quadratic dependence of temperature according to Eq. 1.7. This T^2 behavior of resistivity is then commonly used as a signature of Fermi liquid behaviour.

1

1.2.2 Non-Fermi liquids

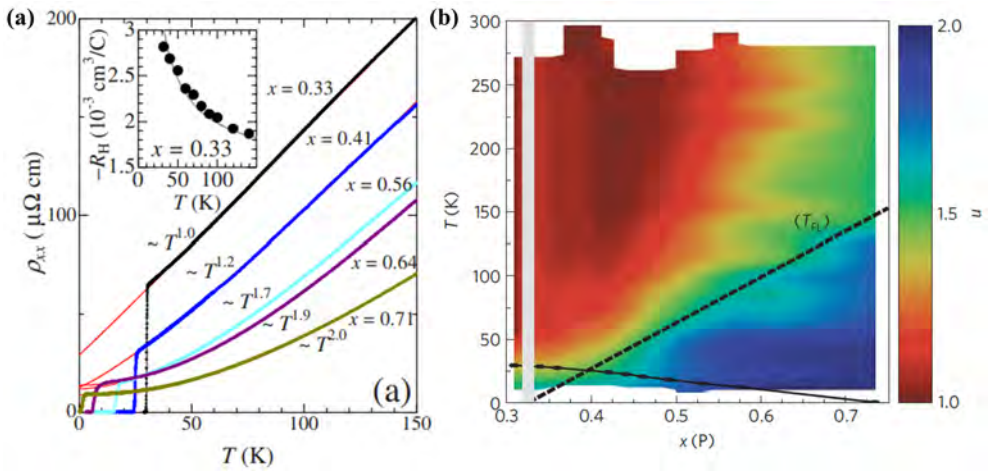

Figure 1.4: *(a) In-plane resistivity of $BaFe_2(As_{1-x}P_x)_2$ for x=0.33, 0.41, 0.56, 0.64, and 0.71 at low temperatures. The fit of $\rho(T)$ to power law illustrate the different temperature dependence for different doping levels. (Reprinted with permission from Ref. [20]) (b) Colour plot of the power-law dependence n as a function of temperature and doping in $BaFe_2(As_{1-x}P_x)_2$. (Reprinted with permission from Ref. [21])*

Since its development, Landau's Fermi liquid theory has been very successful in explaining many fantastic phenomena observed in many-electron systems. However, the discovery of an extraordinary linear-T dependence of resistivity in the normal state of cuprates (a class of compounds displaying high-T_c superconductivity, see next section) made researchers realize the fermion quasiparticle hypothesis may be inappropriate in some systems with strongly interacting electrons. It is worthwhile to note the linear-T dependence of resistivity in cuprates is purely electronic in origin [18, 22], and thus, essentially different with that arising from the usual electron-phonon scattering at high-T, as this anomalous linear behavior can extend

to an ultra-low temperature range, in which neither the conventional Bloch formula or Landau Fermi liquid theory would predict such a dependence.

More interestingly, further research had revealed other powers, with $1 \leq n < 2$ in T^n (e.g $T^{4/3}$ and $T^{5/3}$) of resistivity at low temperatures. To distinguish from Landau's picture of Fermi liquid, the materials with T^n (n≠2) dependence of resistivity are named as "non-Fermi liquids (NFL)". In recent years, many theories were proposed to explain the origin of NFL behaviour. Among them, a widely accepted explanation is the proximity to a quantum critical point (QCP), at which a second-order phase transition (critical point) occurs at absolute zero [15, 18]. The fluctuations of the order parameter (typically the magnetization or the staggered magnetic moment) known to drive the critical phase transitions are held responsible for the change of T-scaling of the resistivity. As shown in Fig. 1.3, in contrast to other phase transitions driven by thermal-related parameters, QCP's are induced by other parameters, such as hydrostatic pressure, magnetic field, or doping [23]. Control of these parameters allows the modulation of a material from FL to NFL. For instance, a continuous modulation from normal FL-like T^2 dependence to NFL-like T-linear dependence of resistivity can be achieved in single-crystalline $BaFe_2(As_{1-x}P_x)_2$ by tuning the doping levels of P atoms [20], as shown in Fig. 1.4. Like the cuprates, these compounds also become superconductors at lower temperatures.

1.2.3 Superconductors

Although the present thesis does not deal with superconductivity, Mott-insulators share some features with superconductors and we will often refer to them, so we will shortly introduced them here.

In ordinary metals, the resistivity decreases gradually with decreasing temperature and always approaches a finite limit near to absolute zero because of the effect of impurities (see Eq.1.5). However, this lower limit is absent in the materials known as superconductors. When the temperature is decreased below a "critical" value (T_c), an abrupt drop of resistivity to zero is observed in these materials. This phenomenon was firstly observed in solid mercury by Kamerlingh Onnes in 1911 [24]. It is no surprising to point out that superconductors have attracted great interests in the past century not only because they are early examples of the realization of macroscopic quantum states but also for their predictably game-changing applications (the possibility to conduct electricity without losses). So far, superconductivity has been found in a wide variety of materials, including simple elements, metallic alloys, and heavily-doped semiconductors. Unfortunately, the transition temperature of all these known superconductors is still too low to be used without additional cooling. For instance, in the *so-called* high-T_c superconductors, like the cuprates and iron-based materials (see Fig. 1.4), the range of transition temperature at atmospheric

pressure only extends up to 150 K, which is still far below room temperature. The quest for achieving room temperature superconductivity at ambient pressure needs a good understanding of the underlying physics behind this attractive phenomenon.

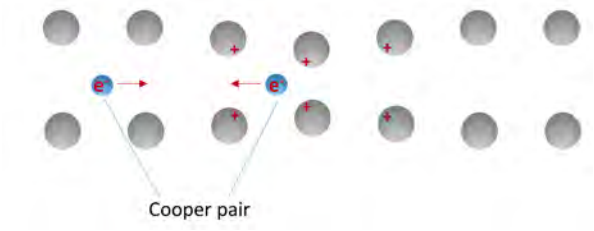

Figure 1.5: *Schematic diagram of the formation of a Cooper pair via the electron-lattice interaction.*

Since the discovery of superconductivity, much progress has been made from both the theoretical and experimental sides. In the traditional Bardeen–Cooper –Schrieffer (BCS) theory, these scientists proposed that the electrons in the superconducting state bind into *Cooper pairs* under attractive potentials rather than moving independently or repelling each other, like in the metal state. The electron-phonon interaction is generally regarded as one of the possible potentials for the formation of Cooper pairs in some conventional superconductors. This can be understood in the case of strong electron-phonon interactions, by the motion of an electron leading to local deformation of the lattice. As a result, another electron is attracted by this small excess of positive charge and forms a correlated pair with the initial electron. In contrast to the isolated electrons in metals, which behave as fermions, the Cooper pairs of electrons act like bosons (with integer spin quantum number and not subjected to Pauli's exclusion principle). This means they can condense into the same quantum state with slightly lower energy, giving rise to an tiny energy gap (of the order of 1 meV). Below T_c, where the thermal energy is less than this superconducting energy gap, the material exhibits zero resistivity. Moreover, except for electron-phonon interactions, other type of interactions can also give rise to a superconducting gap.

Another crucial factor is spin. In the parent compounds of cuprates (like La_2CuO_4 for $La_{2-x}Ba_xCuO_4$), each Cu^{2+} ion possesses an odd number of electrons and therefore displays a net spin of 1/2 and a antiferromagnetic order. After doping with Ba, the introduced hole combines with the Cu^{2+} ion, forming a combination with even number of electrons and no net spin. Researchers supposed that this combination of ions and holes in the CuO_2 planes, which generates a disturbance to the magnetic order of surrounding Cu^{2+} ions, is the real reason for the pairing. Since then, a lot of efforts were made to exploit superconductivity in other systems with similar planes containing spin-1/2 ions. Most recently, by mimicking the electronic config-

uration of cuprates, Li $et\ al$ [25] created a robust superconducting ground state in infinite-layer nickelates and hole doping ($Nd_{0.8}Sr_{0.2}NiO_2$). This infinite layer phase can be obtained from the nickelate perovskite phase, by removing a full plane of oxygen atoms on Nd-O layers. However, a fully understanding of superconductivity in this new member of superconductors, especially in consideration of their absence of magnetic order, is still a mystery for physicists.

1.2.4 Bad metals, strange metals and Planckian metals

According to our basic definition explained above, a metal is a material that shows an increased resistivity with increasing temperature, which arises from the progressive reduction of ℓ (or relaxation time τ) in a severely vibrating lattice. However, the ℓ can never become smaller than the distance between neighbouring atoms (a). Hence, from the viewpoint of our standard understanding of conduction, the increase of resistivity with temperature cannot survive indefinitely. This upper limit in resistivity of normal metals is named as the Mott-Ioffe-Regel (MIR) limit, the value of which can be estimated from Eq. 1.4 by replacing ℓ with a. For simple metals like Cu (see Figure 1.6a), this limit can not be directly observed as their ℓ is nearly two (or even three) orders of magnitude larger than a. In this case, regardless of the drop of ℓ at high temperature, it is still well above the separation of atoms even at the melting temperature [26]. In other metals, such as transition metals and transition-metal compounds, the decay of ℓ is much faster and the resistivity can approach the MIR limit for attainable temperatures. As shown in Fig. 1.6(a), the resistivity of Nb and Nb_3Sb shows a clear saturation at high and ultra-high temperatures, respectively, and the maximum measured values are well below the MIR limit (marked with horizontally dotted lines), validating the standard understanding of conduction.

However, this understanding evolved after the emergence of high-T_c cuprates in the 1980s. Researchers found the increase of resistivity in these materials (especially in non-optimally doped cuprates) can easily surpass the MIR limit, as summarized in Fig. 1.6(b). Subsequently, other materials, like FeAs-based pnictides, alkali-doped fullerenes, vanadium dioxide, and ruthenates, were also reported to violate the MIR condition. Surpassing this limit implies such large scattering rates ($1/\tau$) that, according to Heisenberg's principle (uncertainty of a particle's energy is inversely proportional to its lifetime), if electrons are scattered too quickly, the uncertainty in the energy disqualifies them as coherent quasi-particles [27–29]. This leads to the absence of a sharp Drude peak in the optical conductivity, which is a distinct characteristic of normal metals. Due to their obviously different performance compared to normal metals at high-T, these metallic materials violating the MIR limit are called as *bad metals*.

In addition to satisfying the MIR limit at high-T, the resistivity of normal met-

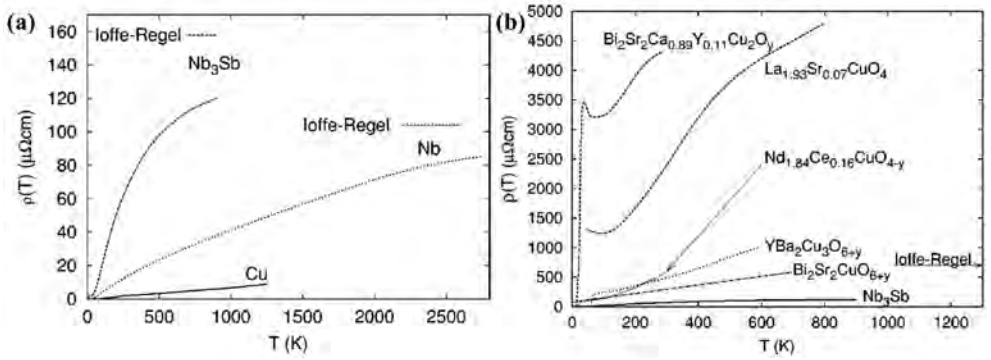

Figure 1.6: *Resistivity of various metals as a function of temperature. (a) Resistivity saturates upon approaching the Ioffe-Regel limit (also known as Mott-Ioffe-Regel or MIR limit) in simple metals and transition metals. (b) Absence of saturation in a series of cuprate superconductors. (Reprinted with permission from Ref. [26])*

als is also characterized by its Fermi-liquid-like T^2 dependence at low-T. In some electron correlated systems known as *strange metals*, a linear dependence of the resistivity is instead observed at low-T. This emergent phenomenon, firstly discovered in optimally-doped cuprates [30, 31] and subsequently reported also in other strongly correlated systems (e.g ruthenium oxides [32], organic conductor [33], heavy-fermion metals [34], and magic-angle graphene [35]), has become one of the long-standing puzzles in condensed matter physics. Although a general consensus about its origin is still absent, recent studies have proposed that the electrons in a strange metal behave as a fluid ruled by the laws of hydrodynamics, with a minimum viscosity determined by $\hbar$, and proportional to the entropy [29]. Because entropy is very small at low temperatures, strange metals can show low, *good metal*, resistivities at low temperatures; while displaying *bad metal* resistivities at high temperatures. That hydrodynamics rules implies that the crystal lattice becomes irrelevant in these systems. Indeed, the determining length scale (equivalent to the mean free path in the quasiparticle Drude formalism) is the length scale of the quenched disorder. However, in spite of the presence of significant disorder, the resistivity is low at low temperatures because of the small viscosity of the electron fluid. Surprisingly, the simple formalism describing the conductivity of these strange metallic systems as "compressible quantum matter" [29] is similar to that used to describe the physics of black holes [36].

It has been shown that the T-linear behaviour found in strange metals is likely to associate with a universal Planckian bound in their scattering rate ($\Gamma = 1/\tau$) [29, 31, 32, 35] :

$$\frac{1}{\tau} = \alpha k_{\mathrm{B}} T/\hbar \tag{1.8}$$

where α is a dimensionless constant close to 1, k_B is the Boltzmann's constant, and $\hbar$ is the reduced Planck's constant. To distinguish them from other metallic systems, metals that satisfy the universal Planckian dissipation law, are also referred to as *Planckian metals*.

1.3 Conduction in non-metals

As discussed in Section 1.1, a solid can be defined as metal or non-metals depending on how the energy states within the electronic bands are occupied by electrons. An electrical insulator is then a system in which, at zero temperature, all energy bands are either completely filled with electrons or completely empty. Theoretically, the distribution of the velocities of electrons in the fully occupied bands cannot be changed so that, they make no contributions to the flow of charge [37]. Hence, non-metals possess no conductivity at zero temperature. Measurable conductivity of non-metals at non-zero temperature can arise in some materials from the hopping of the highest energy electrons (at the top of the valance band) to an empty state at the bottom of the conduction band, where they can contribute to the conductivity. According to the Fermi-Dirac distribution (Eq. 1.3), the probability for electrons to be promoted to a particular energy ϵ, is determined by the energy gap between the valence band and conduction band (ϵ_{g}) and the temperature, and is proportional to $\exp(\epsilon\text{-}\epsilon_{\mathrm{g}})/k_{\mathrm{B}}T$. Accordingly, measurable conduction only takes places in materials with a band gap below 3 eV, called semiconductors, which are the foundation of modern electronics (*e.g* transistors and integrated circuits).

Due to their distinct band structure with metals, the impurities usually exert a very different effect on the conductivity of semiconductors, compared to their effect on metals. Normally, defects in metallic solids work as scattering centers, impeding the flow of electrons and damaging conductivity. On the contrary, properly-chosen impurities in semiconductors form an energy level inside the energy gap, so that either electrons in these levels will need less energy ($\epsilon \ll \epsilon_{\mathrm{g}}$) to reach the conduction band increasing the electron conductivity or, in the case of defect levels closer to the valence band, the electrons from the valance band can occupy that level with relatively little energy ($\epsilon \ll \epsilon_{\mathrm{g}}$), increasing the hole conductivity. These two scenarios as known as n-doping and p-doing, respectively. This change in the energy levels, modifies the Fermi energy of the material, which moves close to the bottom of the conduction band for an n-doping and close to the top of the valence band for p-doping. As a consequence of the exponential dependence of the density of electrons

with ϵ_F, doped semiconductors show a much enhanced conductivity with respect to intrinsic semiconductors.

However, in non-metals, it is also possible to observe conduction without promoting electrons to the conduction band. If the material contains a fair amount of disorder with a large number of relatively deep defect levels, electrons associated to those defects can hop from one defect site to another. This happens, for example, in oxides when oxygen vacancies (and their associated electrons) are present. Electron or hole hopping, gives rise to different energy and temperature dependence compared to those of observed for conduction band transport.

The characterization of the transport mechanisms in non-metals begins with experiments on electrical properties. Among them, the most representative one is their negative temperature coefficient of resistivity, significantly contrasting to metals. The possibility of charge transport by hopping makes that, when it comes to the real cases, the temperature dependence of resistivity in non-metals can be different depending on the distribution of defects. Over the last two centuries, a wide variety of theories had been proposed [38–43]. Here, limited by the scope of the thesis, we only introduce two commonly used models: Nearest Neighbor Hopping (NNH) and Variable Range Hopping (VRH).

1.3.1 Nearest Neighbor Hopping

In the scenario of NNH conduction, electrons with activation energy (W) are supposed to hop from the top occupied sites to the nearest neighboring empty sites. The corresponding probability of success in a hopping attempt at a specific temperature can be estimated by the following equation [44, 45]:

$$P(T) = \nu_{ph} \exp(-\frac{2R}{\xi} - \frac{W}{k_B T}) \tag{1.9}$$

where ν_{ph} indicates the phonon frequency associated with the hopping process and the factor $\exp(-2R/\xi)$ represents the wavefunction overlap of two states with localization length ξ and separation distance R. The value of R is directly linked with the orbital degeneracy (N_d), which characterizes the number of different states for a particular energy level, in the form shown below:

$$R = (\frac{4\pi N_d}{3})^{1/3} \tag{1.10}$$

Using the estimated probability of the hopping process, if the actual distribution of electrons among the available energy levels of the partially-filled bands (density of states (DOS) or g(E)) is already known, the temperature dependence of conductivity originating from the NNH mechanism can be determined by:

$$\sigma(T) = \frac{1}{6} g(E) e^2 r^2 P(T) = \frac{1}{6} g(E) e^2 R^2 \nu_{ph} \exp(-\frac{2R}{\xi} - \frac{W}{k_B T}) \tag{1.11}$$

For simplification, Eq. (1.11) is usually written in the Arrhenius form:

$$\sigma(T) = \sigma_0 \exp(-\frac{W}{k_B T}) \tag{1.12}$$

the NNH mechanism has been reported to be dominant in many conventional semiconductors, especially in the intermediate temperature range (100- 400 K).

1.3.2 Variable Range Hopping

The hopping process is significantly dependent on the local distribution of defect sites. The NNH regime is valid only if the hopping distance is limited to the spatial nearest site. However, this condition has been found to be broken at correspondingly low temperature in which the hopping electron cannot find an energetically favorable position in the spatial nearest sites. Alternatively, the electrons hop to the sites that are remote in space but closer in energy. This type of hopping of electrons is known as Variable Range Hopping (VRH) and was introduced by Mott in 1968 [43].

In the VRH regime, the hopping of electrons originating from one site is still dominated by the hop to another site at closest range. However, this closest range is localized in the four-dimensional space (three spatial coordinates and one energy coordinate) after considering the combined effect of R and W. In real space, the directions of these hops will be random. The average hopping probability in the four-dimensional space is approximated by $P \simeq \exp(-\overline{\Re})$, with $\overline{\Re}$ representing the average nearest neighboring hopping range. At this point, the critical factor in calculating the VRH conductivity is the determination of $\overline{\Re}$. If the contribution of the applied electric field to the hopping is negligible, the $\overline{\Re}$ is given by [46]:

$$\overline{\Re} = \frac{3}{4} (\frac{3\xi}{2\pi g(E) k_B T})^{1/4} \tag{1.13}$$

Or in a simplified form:

$$\overline{\Re} = (\frac{T_o}{T})^{1/4} \tag{1.14}$$

According to Eq. (1.11), the conductivity in the VRH regime can be written as:

$$\sigma = \sigma_0 (-\frac{T_o}{T})^{1/4} \tag{1.15}$$

with

$$\sigma_0 = \nu_{ph}(\frac{g(E)\xi}{\pi k_B T})^{1/2} \tag{1.16}$$

It is worthwhile to note that the exponent $1/4$ in Eq. 1.15 is only valid in a three-dimensional system. For one-dimensional and two-dimensional systems, $1/2$ and $1/3$ should be used, respectively. However, as pointed out by Efros and Shklovskii (ES) in 1975 [38], a gap in the density of states (DOS) near the Fermi level would be created under the Coulomb interaction between localized electrons and this Coulomb gap was supposed to have an important effect on the conductivity at low temperatures. As a result, the conductivity follows a $-1/2$ scaling of temperature in all dimensions ($\sigma \sim T^{-1/2}$). This type of conduction model is called Efros-Shklovskii variable range hopping (ES VRH).

By extending the measured temperature range, various types of hopping processes may be observed in the same material. Fig. 1.7 shows the conductivity data of a-Si:Se:H film at different temperatures [47]. The conductivity above 365 K was plotted in Fig. 1.7(a) as a function of $1000/T$. The robust linear dependence manifests the NNH process is dominant in the conduction in this high temperature regime. On the contrary, the conductivity data below 365 K follows the Mott VRH model, indicating a crossover between these two mechanisms at the mentioned temperature. Moreover, in highly disorder systems, crossover between Mott VRH to ES VRH regimes has also been observed [48].

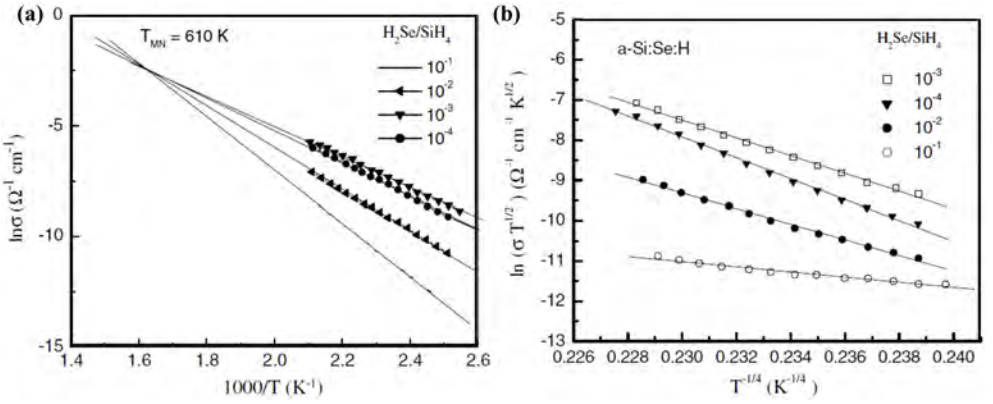

Figure 1.7: *Extrapolated plot of lnσ versus $1000/T$* ***(a)*** *and ln ($\sigma T^{1/2}$) versus $T^{-1/4}$* ***(b)*** *of a-Si:Se:H film in different dopant concentration in different temperature regimes. (Reprinted with permission from Ref. [47])*

1.4 Metal-insulator transition

A detailed discussion of the difference between metals and non-metals in terms of band structure and temperature dependence of resistivity is given in the above sections. However, the qualitative definition of a material as metal or insulator may only be true under specific conditions. Change of external parameters, such as pressure, stress, magnetic field, gate voltage and temperature, or internal degrees of freedom, such as atomic sizes and composition, may induce a sudden change in conduction behaviour from a metallic state to insulating state, or vice versa. This phenomenon is denoted as "metal-insulator transition (MIT)". Well-known systems exhibiting metal-insulator transition are the strongly correlated oxides. These systems have complex phase diagrams with many different phases as a function of temperature and composition. This complexity arises from the presence of competing interactions of similar magnitude, which give rise to subtle energy balances that can be drastically change with small changes in temperature, composition, pressure of electric and magnetic fields. Some of these phases have metallic nature and some have insulating nature. Thus, these systems lead often to metal-insulator transitions. Famous examples are V_2O_3, Fe_3O_4, the $La_{1-x}A_xMnO_3$ system (where La is substituted by different amounts of alkaline earth metals Sr or Ca), or the $ReNiO_3$ system, central subject of this thesis, where Re is a rare earth atom. The metal-insulator transition, triggered at a temperature T_{MI}, is usually accompanied by structural or/and magnetic phase transitions.

Numerical theories have been proposed to describe the underlying mechanism behind these intriguing phenomena, however, metal-insulator transition is still one of the least understood problems in condensed matter physics. The difficulty arises from the qualitatively distinction between metals and insulators, which are completely different physical systems with very different elementary excitations [49]. Therefore it is easy to imagine how complicated the dynamic process will be in the intermediate regime, during the phase transition. Here, conventional band theory approaches proved of little help. In the following we briefly introduce some ideas on how the metal-insulator transition can take place in narrow-band systems, such as transition metal (TM) compounds and other strongly correlated oxides.

1.4.1 Mott-Hubbard insulators

As predicted by classical band theory (see Fig. 1.1), materials with partially filled bands should exhibit a good metallic behavior. However, this criterion was proved to be inappropriate in TM compounds with partially filled d or f orbitals (narrow energy bands). Early works by Slater proposed the anomalous insulating behaviour of TM compounds arouse from a gap opened by the antiferromagnetic ordering [51].

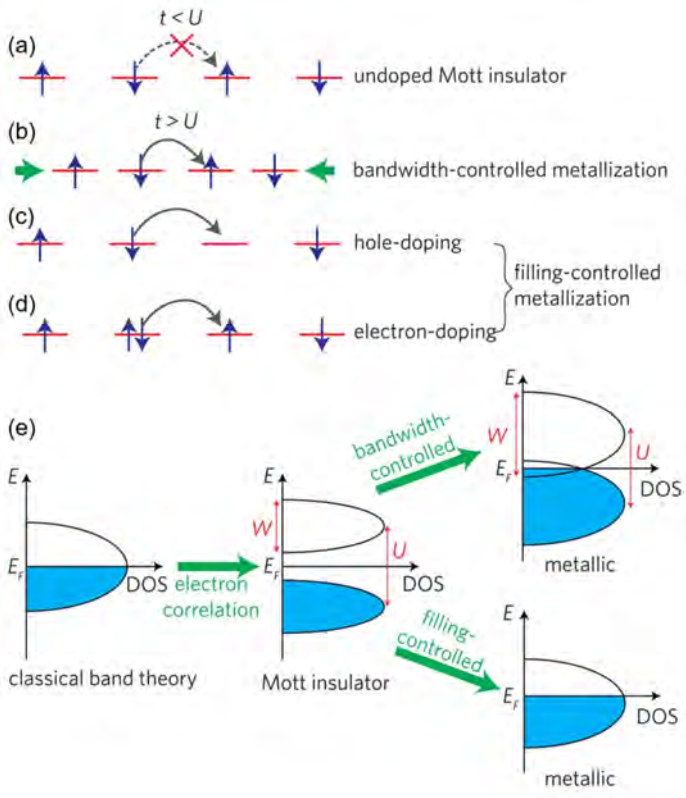

Figure 1.8: *Mechanisms responsible for the Mott-Hubbard insulator. (a) The inhibition of electron hopping in Mott insulators by Coulomb repulsion U. (b) The increase of delocalization energy t by compressing the lattice, which leads to a transition from insulator to metal when $t > U$. (c) and (d) The hole/electron doping induces empty/doubly-occupied sites and gives rise to a filling-controlled metallization. (e) The electronic band evolution during metal-insulator transition in Mott insulators. (Reprinted with permission from Ref. [50])*

Latter on, this approach was also ruled out as the insulating behavior in some TM compounds was found to remain at temperature well above the Néel temperature ($T_{\text{Néel}}$) (the paramagnetic-antiferromagnetic transition temperature). Since then people realized this problem could not be clarified in the framework of classical band theory without substantial modifications.

The first attempt was made by Mott in 1949 [52, 53] and was demonstrated to be correct by subsequent researches. In the classical band theory picture, electrons are approximately treated as itinerant particles moving independently from other electrons in an effective periodic potential [50]. This approximation is expected to be

satisfied only when the electron's kinetic energy is sufficiently larger than other energy scales in the problem [49]. Mott argued that the Coulomb repulsion energy, U, between electrons occupying the same sites in TM compounds is even stronger than their kinetic energy (see Fig. 1.8(a)). This is partially because the strong repulsion of the electrons due to the narrow energy bands in these TM compounds inhibits delocalization of electrons. The predicted "partially filled band" in these TM compounds splits into a fully-filled lower Hubbard band (LHB) and an empty upper Hubbard band (UHB) instead, as shown in Fig. 1.8(e). The energy gap between these two bands is determined by the U. As a consequence, this class of materials (named as Mott-Hubbard insulators) are insulating rather than conducting.

Moreover, the strong correlation of electrons in the narrow energy bands also renormalize the mass of charge particles. The reason is that the electron-electron correlation effectively increases the inertia of the electrons to the change of velocity, which can be expressed as a change of the bare mass of free electrons (m_0) by the effective mass of quasiparticles (m^*). According to the Brinkman-Rice model for correlated electrons ($m^*/m_0 = (1-(U-U_0))^{-1}$) [54], when the U approaches a limit value U_0 at which a correlation gap opens at the Fermi level, the effective mass shows an enhancement. Hence, the mass divergence is also a signature of Mott-Hubbard insulators.

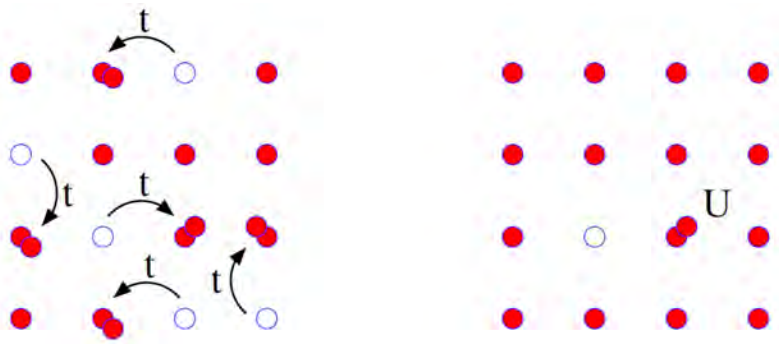

Figure 1.9: *Illustration of the terms in the Hubbard Hamiltonian. Left: The electron kinetic energy t. Right: The on-site electron repulsion U. (Reprinted with permission from Ref. [55])*

Inspired by Mott's ideas, in 1963 Hubbard introduced the Coulomb repulsion into the Hamiltonian and then the energy of the system can be described as [56, 57]:

$$H = -t \sum_{(i,j),\sigma} c^{\dagger}_{i,\sigma} c_{j,\sigma} + U \sum_{i} n_{i,\uparrow} n_{i,\downarrow} \tag{1.17}$$

known as the Hubbard Hamilonian, where the first term represents the kinetic energy of the system (or the intersite hopping of electrons) and the second one indi-

cates the effect of the onsite electron repulsion. Among all the parameters, the t is the hopping integral which is determined by the overlap of two wavefunctions on the pair of atoms involved in the hopping process. Usually, the ratio t/U (or U/t in some works) is used to characterize the competition between the kinetic energy and the interaction energy of electrons. The $c^{\dagger}_{i,\sigma}$ and $c_{j,\sigma}$ describes the creation and destruction operators for an electron of spin σ, while $n_{i,\sigma}$= $c^{\dagger}_{i,\sigma}$ $c_{j,\sigma}$ are the number operators. It is worth to note that the Hubbard Hamiltonian only considers the interaction between two electrons (with opposite spin because of Pauli's principle) on the same site as they have the largest value of U. The expression $n_{i,\uparrow}$ $n_{i,\downarrow}$ describes this property. Fig. 1.9 illustrates the hopping of electrons from one site to the other site (left) and the repulsion of electrons on the same site (right).

1

1.4.2 Charge-transfer insulators

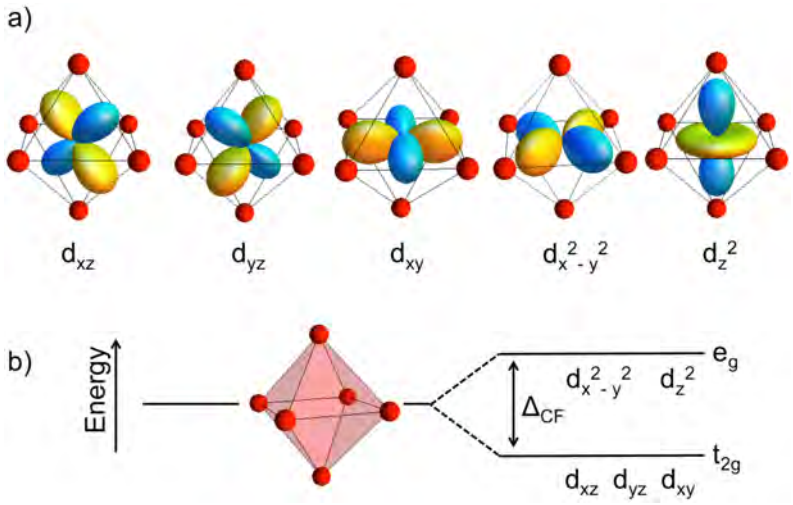

Figure 1.10: *Representation of the 3d orbitals. (a) 3d orbitals with their 5 distinct wave functions with colors (blue and yellow) characterizing different sign or phase. The positions of the ligand oxygen atoms are marked in red. (b) Crystal field splitting in 3d orbital. The $d_{x^2-y^2}$ and d_{z^2} orbitals, which point toward the ligand oxygen atoms, are lifted in energy due to the octahedral crystal field (CF) splitting. (Reprinted with permission from Ref. [57])*

The Mott-Hubbard model, which takes only the d-d orbital excitations into account, is a great improvement in describing the electric conduction of transition metals in comparison with the Bloch model. Whilst for some TM compounds with perovskite ABO_3 structure, the transition metals ($e.g$ Cu and Ni) located on the B sites

are so close to the surrounding oxygen atoms that the interaction between them cannot be neglected. More specifically, the d orbitals of transition metals have a orbital momentum equal to 2 and therefore possess five different wave functions, indicated in Fig. 1.10(a). Among them, the $d_{x^2-y^2}$ and d_{z^2} orbitals are pointed toward the oxygen atoms, while other three orbitals (d_{xz}, d_{yz} and d_{xy}) occupy the space between two neighboring oxygen sites. Due to the repulsion with the electrons in the oxygen anions, the d orbitals directly oriented towards the oxygen atoms are lifted in energy, leading to a so-called crystal field splitting, as shown in Fig. 1.10(b). The former two orbitals are usually called e_g band and the latter three orbitals with lower energy form a t_{2g} band.

Distinct from the d-d excitation in M-H insulators, the electrons in these insulators hop from the oxygen p band to the transition metal d band instead. The energy gap between these two bands are referred to as the charge-transfer gap (Δ). As a result of the electron hopping, a ligand hole L is created at the oxygen orbital and correspondingly, the electron counting on the transition metal d orbital is increased to n+1, as:

$$d^n \rightarrow d^{n+1}L \tag{1.18}$$

This type of transfer of electrons from anions to cations is not considered by the M-H model. In order to distinguish them from the M-H insulators, the insulators caused by the interaction between transition metals and neighbouring oxygens are usually known as *Charge transfer (C-T) insulators*.

The intriguing phenomena discovered in M-H and C-T insulators have revolutionized our understanding of conduction. In the model established by Zaanen, Sawatzky and Allen (ZSA) [58], for materials in which both mechanisms are possible, both the U and Δ are considered crucial in regulating the electronic structure of TM compounds; while they are considered as competing entities. The distinct band structures of a M-H insulator and a C-T insulator are illustrated in Fig. 1.11. According to the ZSA diagram, whether a material is Mott-Hubbard insulator or charge-transfer insulator depends on the relative magnitude of U and Δ. When $U > \Delta$, the material is referred to as M-H insulator; otherwise, it is a C-T insulator.

However, latest researches pointed out that the ZSA scheme also cannot explain the electronic behavior of all TM compounds. Physically, the value of Δ is inversely proportional to the valence of the TM ions [59]. To some TM compounds like $NaCuO_2$ and $CaFeO_3$, the unusually high valence of Cu^{3+} and Fe^{4+} is expected to induce a nearly-zero or negative Δ and, therefore, should be metals. Surprisingly, they are insulating instead, manifesting the breakdown of the positive charge-transfer regime. This new type of compounds with a negative Δ are named as "*Negative charge-transfer insulators*". The Rare-earth nickelates ($RENiO_3$) investigated in this work belong to such region of the ZSA diagram.

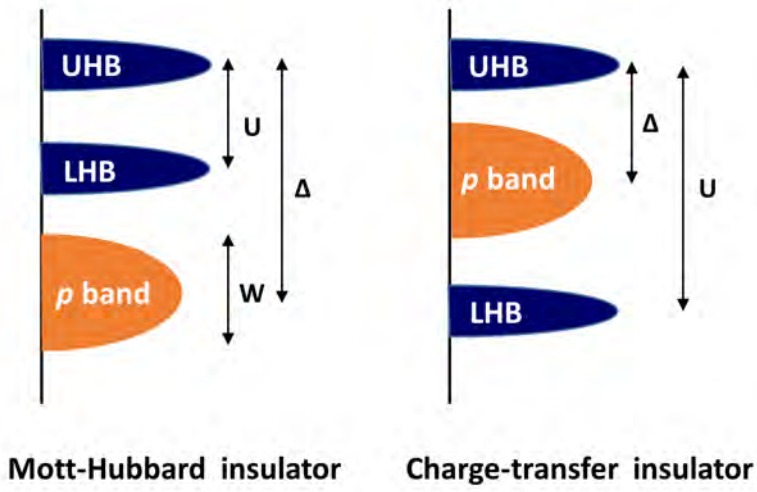

Figure 1.11: *Schematic band structure of (a) a Mott-Hubbard insulator and (b) a charge-transfer insulator. The U represents the Coulomb repulsion, Δ describes the charge-transfer gap between the transition metal d band and the oxygen p band. W is the bandwidth of p band.*

1.4.3 The phase transition

As we mentioned at the beginning of this section, the conduction behavior of a material can be modulated by changing some external or internal parameters. In some interesting cases exposed above, a sudden transition from insulating state to metallic state (metal-insulator transition or MIT) can happen. This is commonly observed in both the M-H insulators and C-T insulators. In these TM compounds, although the d-d Coulomb repulsion or p-d charge transfer induce an unexpected insulating state, the energy gap U or Δ is relatively narrow. When the kinetic energy (t) of the electrons becomes comparable with the relevant gap, the MIT occurs. For instance, by compressing the lattice (e.g applying pressure or stress) of TM compounds, the bandwidth ($W = 2zt$) will be increased and leads to an overlap between LHB and UHB in M-H insulators or an overlap between p-band and UHB in C-T insulators. This type of driven MIT is referred to as bandwidth-controlled MIT. In order to compress the lattice, "chemical pressure" can be exerted by replacing the A cation by a large one and that is why composition is often a key parameter in determining the MIT.

Another commonly used way to induce MIT is by doping the lattice with charge carriers (named as "filling-controlled MIT"). Distinct from the former case, filling-controlled MIT is achieved by modifying the effective values of U and Δ (see Fig.

1.8(c-e)). It is worth to note the MIT phenomena in most works is observed in the process of cooling or heating the specimens. That is because the change of temperature in these complex compounds in which the TM ions are subjected to various competing (close in energy) interactions usually brings about a change in the phase stability, that can be associated to an electronic band opening. In these sense, the temperature-driven MIT is equivalent to a bandwidth-controlled MIT. We will discuss in details about this kind of MIT in the next section by employing $RENiO_3$, the subject of this thesis, as an example.

1.5 Rare-earth nickelates

The story of perovskite rare-earth nickelates ($RENiO_3$) began in 1971 when they were firstly synthesized by Demazeau *et al* [60]. Note the synthesis of the perovskite phase in this material requires high pressures and it is usually hard to reach in the lab. No single crystals were reported and only polycrystalline (ceramic) samples were available. After that, they almost vanished from the view of researchers for more than 20 years [61]. Fortunately, this class of oxides, which is very popular in recent years, have regained interests since the development of techniques for thin-film deposition and also the discovery of high-T_c superconductivity in other similar oxide systems, like cuprates, manganites, and iron pnictides. Today, after having been studied for half a century, $RENiO_3$ have proved themselves as a very interesting case in clarifying many concerns in condensed matter physics.

$RENiO_3$ are electron correlated TM compounds with perovskite structure, in which the RE cations occupy the A sites and are surrounded by the NiO_6 octahedra. Note the RE in the formula of $RENiO_3$ represents a family of rare-earth atoms, such as La, Pr, Nd, Sm,..., Lu. Regardless of their rich landscape of physical properties, the most famous characteristic of $RENiO_3$ (RE $\neq$ La) is a sharp metal to insulator transition, which is triggered when the system approaches the transition temperature T_{MI}.

Remarkably, as a negative C-T insulator, the electronic structure of $RENiO_3$ is determined by the wavefunction overlap between the Ni and O orbitals and, therefore, their T_{MI} can be continuously modulated by deforming the NiO_6 octahedra. This can be achieved by varying the RE ion, applying hydrostatic pressure or, in the case of epitaxial films, by altering the lattice mismatch between film and substrate or the film thickness.

1.5.1 Phase diagram

A well-known phase diagram shown in Fig. 1.12 illustrates the phase transitions of $RENiO_3$ family as a function of temperature and Ni-O-Ni angle. The Ni-O-Ni angle

describes the tilting of octahedra in the lattice and is determined by the radius of A-cations (r_A). At high temperature or large Ni-O-Ni angle, $RENiO_3$ display metallic behavior with a paramagnetic phase. Except for an extreme case with RE= La, all other nickelate compounds adopt an orthorhombic configuration in the metallic phase. Bulk $LaNiO_3$, which possesses the biggest A-cations, has a rhombohedral crystal structure and this metallic and PM phase is found to be retained in the whole temperature range (*Note*: a MIT is also reported in ultra-thin $LaNiO_3$ films [62]). On the contrary, other $RENiO_3$ transform to a insulating phase below T_{MI}, which is driven by a structural phase transition from orthorhombic to monoclinic symmetry. Moreover, the value of T_{MI} shows a clear evolution with the Ni-O-Ni angle. For a perovskite with a smaller A-cation, the surrounding octahedra tend to tilt more towards A site to minimize the occupied space, giving rise to a smaller Ni-O-Ni angle. Consequently, the overlap between the Ni d-orbitals and O p-orbitals is also reduced, promoting the insulating phase. For instance, the $LuNiO_3$ with the smallest A-cations exhibits a highest $T_{MI} \simeq$ 600 K, which is almost 500 K larger than that of $NdNiO_3$. Note the difference in ionic radius between Lu and Nd is only about 0.1 Å. Hence, varying the A-cations is often taken as an effective control parameter to modulating the T_{MI} of $RENiO_3$. A very interesting case is the doped $Sm_{0.6}Nd_{0.4}NiO_3$ (or $Sm_{0.5}Nd_{0.5}NiO_3$ in some works) wherein a room-temperature MIT is achieved.

Another interesting feature displayed in the phase diagram is the difference of T_{MI} and $T_{Néel}$ in some of the $RENiO_3$. For $PrNiO_3$ and $NdNiO_3$, the MIT and Néel transition occur simultaneously. Whilst in the rest of nickelates series with $r_A \leq r_{Sm}$, the evolution of $T_{Néel}$ is largely distinct from their T_{MI}. Detailed studies revealed that the Néel transition of these nickelates with $T_{MI} > T_{Néel}$ display a second-order character, while a first-order Néel transition is reported in those with $T_{MI} = T_{Néel}$ [64, 65]. On the contrary, the MIT of all kind of nickelates is believed to be first-order [57]. However, in the extreme case of $LaNiO_3$ which possesses the largest Ni-O-Ni angle and a rhombohedral unit cell (instead of orthorhombic), both the MIT and Néel transitions are absent.

The last feature of the phase diagram which is worth to note is the symmetry-lowering at low temperatures. Accompanied with the electronic transition, a phase transition from high-T orthorhombic phase to low-T monoclinic phase also happens (except for the rhombohedral $LaNiO_3$). Notably, a breathing-mode distortion occurs in the insulating phase wherein the octahedra are alternatively expanded or contracted (see Fig. 1.13(a-b)). In these non-uniform octahedra, two inequivalent Ni sites with different valence Ni cations (Ni^{2+} and Ni^{4+}) and disproportional bond-length are created. In the smaller octahedra, the O-anions are closer to the Ni-cations, leading to a stronger Ni-O hybridization [63]. For the bigger octahedra, the effect on hybridization is opposite. As we will discussed in the next subsection, this bond disproportion is a crucial ingredient for understanding the electronic configuration

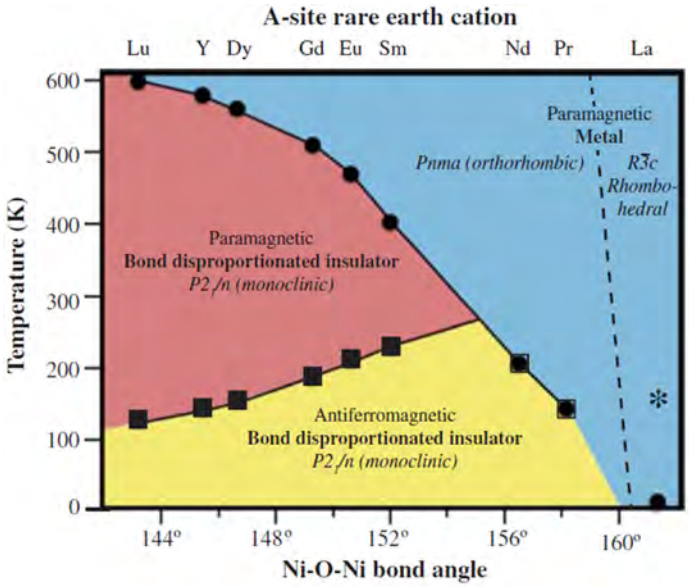

Figure 1.12: *Phase diagram of the $RENiO_3$ family, which illustrates the evolution of the electronic (circle), the magnetic (square) and structural transition with the Ni-O-Ni bond angle and the RE cations. (Reprinted with permission from Ref. [63])*

of insulating nickelates.

1.5.2 Electronic configuration

Among the researches on nickelates, a considerably large proportion of works have been focused on the establishment of their electronic configurations in the ground state. In an extreme case, the Ni-O bonds are perfectly ionic in $RENiO_3$ and the Ni cations should adapt to a valence of 3+ [57]. This is equivalent to a d^7 configuration with 7 electrons distributed among the t_{2g} and e_g orbitals. Lowering the temperature to T_{MI}, a breathing-mode distortion of octahedra is triggered and then facilitates a transition to insulating phase. In this process, the formation of bond disproportionation (with alternating long and short bonds giving rise to larger and smaller octahedra) should also induce a diference in the electronic configurations of neighbouring Ni ions. Initial studies assumed the two inequivalent Ni sites in the insulating phase adopt a charge ordering with alternating $d^{7-\delta}$ and $d^{7+\delta}$ configurations, where the value of δ was found to be directly correlated to the length of the bonds [67, 68].

However, calculations and experiments in recent years have found such an orig-

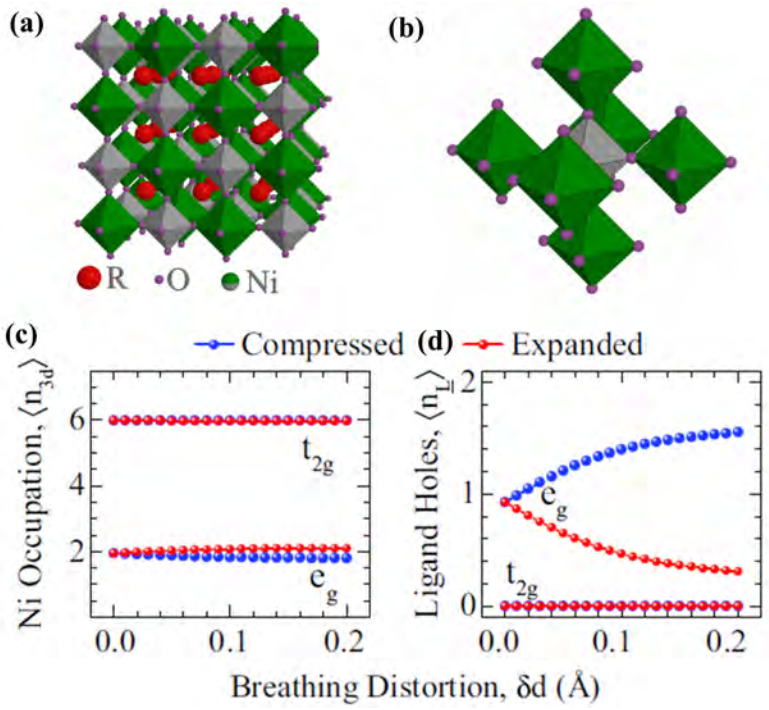

Figure 1.13: *(a) and (b) Extended (green) and contracted (gray) octahedra present in the breathing-mode distorted insulating phase of $RENiO_3$. Distribution of (c) Ni 3d electrons and (d) ligand holes as a function of breathing distortion. (Reprinted with permission from Ref. [66])*

inal scenario to be unlikely [66, 69–72]. The key point of the new picture postulates the Ni sites have a uniform d^8 configuration. Instead of the difference in Ni valence, the bond disproportionation is more likely to induce alternation of the amount of holes in the ligand O p-band. Or in other words, the charge ordering pattern in this new picture resides on O rather than on the Ni sites [73, 74]. As shown in Fig. 1.13 (c-d), a theoretical study by Green *et al.* demonstrated that the total occupation per Ni site is 8 electrons rather than 7 and only a very little change in the Ni 3d occupation occurs via the breathing-mode distortion [66]. Instead, the oxygen orbitals show a very active response to the distortion. For details, the starting point of nickelates in the metallic phase is a d^8L state with one ligand hole per cluster. After the distortion, the holes shift to the contracted octahedra, leading to a d^8L^2 state. Correspondingly, the electronic configurations in the extended octahedra adopt a d^8 state. In particular, such a hypothesis seems to be more reasonable when one considers the change in the Ni valence between the two sublattices will be suppressed by the large

repulsive d-d interaction [69]. And considering the very small or even negative Δ in such systems, it should be more energetically favorable to transfer a hole from Ni to O sites. According to the new picture, the evolution of the electronic configuration of nickelates before and after MIT can be described as below:

$$d^8L + d^8L \rightarrow d^8L^2 + d^8 \tag{1.19}$$

Back to the electrical properties, the splitting of the d^8L band caused by the breathing-mode distortion leaves a energy gap and then gives rise to a insulating phase.

1.5.3 Effect of epitaxial strain

Nowadays, strain engineering has become a commonly used method to tailor numerous properties of materials. Compared with their bulk forms, thin films epitaxially grown on crystalline substrates display richer behaviour and phenomena and therefore have more potential applications. For example, mobility in semiconductors, phase and electrical transition temperatures in correlated perovskites and high-T_c superconductors can be controlled by epitaxial strain [75]. In the case of nickelates, in addition, epitaxial strain allows the synthesis of single crystal nickelates that cannot easily be obtained in bulk. In general, the effect of epitaxial strain on thin films is achieved by subtly altering their crystal structures, with respect to the bulk equilibrium state. More importantly, the applied strain to the film is possible to be tuned either by employing different substrate or by modulating the thickness of the film. The former case is resulting from lattice-matching between the film and the substrate, either at the growth temperature or during cooling after growth, wherein the lattice of the film is compressed or stretched to adapt to the substrate. The in-plane strain that is achieved (ε_{xx}) can be defined as:

$$\varepsilon_{xx} = \frac{a_{sub} - a_{bulk}}{a_{bulk}} \tag{1.20}$$

where the a_{sub} and a_{bulk} are the pseudo-cubic lattice parameters (those of the primitive perovskite unit cell) of film and substrate, respectively. In the latter case, the controlling of strain with thickness is based on the fact that the elastic energy accumulated in the film under strain, increases linearly with thickness and, thus, upon increasing thickness, the possibilities that strain relieving mechanism, such as creation of defects, take place become increasingly favorable. In this thesis, the strain in the nickelate films was mainly tuned by these two methods.

For the case of the $RENiO_3$, the most straightforward and widely investigated result of applying epitaxial strain is the modulation of their T_{MI}. Theoretically, the change of strain state should have an effect on the T_{MI} equivalent to that of altering the RE cations. Correspondingly, the straightening (bending) of the Ni-O-Ni angle

changes the orbital overlap and facilitates the broadening (narrowing) of bandwidth and then forces the T_{MI} shift to a lower (higher) temperature. Indeed, this model has been verified experimentally in systems with tunable compressive strain. As the compressive strain ranges from a nearly-zero condition to a larger value, a clear shift of T_{MI} to lower temperatures has been commonly observed in all monoclinic nickelates. In some extreme cases with very large compressive strain, a single metallic phase without MIT can also be produced in the nickelate films [76, 77].

Apparently, the compressive strain can exert its effect on the structural and electronic properties of nickelates in a relatively direct way. However, the role of tensile strain is still a debated question. In an ideal case, the tensile strain should have a strong influence, opposite to that of compressive strain, on the tilting of octahedra and, therefore, should push the T_{MI} towards higher temperature. Surprisingly, this natural prediction is found to be in contrast to the experimental observations, where the T_{MI} is almost independent of the magnitude of the tensile strain [57]. The most possible explanation for this anomalous behavior is the introduction of oxygen vacancies by large tensile strain. Theoretical works revealed that the formation energy of oxygen vacancies in nickelates is significantly lower than other perovskite systems, like $SrTiO_3$ [78]. Note that the oxygen vacancies induce a lattice expansion in perovskites due to the new balance of Coulomb interactions and, therefore, the presence of oxygen vacancies removes the need for the film to relax the tensile strain. Therefore, forming oxygen vacancies is energetically more favorable in nickelate films with large tensile strain, as discussed by Conchon $et\ al$,[79]. As the formation of oxygen vacancies only has a negligible effect on the tilting of octahedra, the increase of tensile strain does not result in a clear increase of T_{MI}. But the oxygen vacancies can cause the localization of electrons and then lead to a serious drop of conductivity. Indeed, a great enhancement of resistivity is observed in the nickelate films under tensile strain.

Moreover, detailed characterizations indicate the orbital polarization of Ni can also be affected by the strain [77, 81]. In the metallic phase of nickelates, the Ni^{3+} ions adopt a d^8L electron configuration with partially filled e_g^2 orbital. And the e_{g} orbitals have two different symmetries: $3z^2$-r^2 and x^2-y^2 (see Fig. 1.10). As shown in Fig. 1.14, these two symmetries are degenerated in the unstrained system; whereas the degeneracy is found to be clearly broken in the films with strain, causing a polarization of e_{g} orbitals. Due to the distinct changes in the overlap of the different orbitals under in-plane compression or expansion, both the compressive and the tensile strain contribute to the polarization but in a completely different way. Specifically, the tensile strain declines the energy of the x^2-y^2 orbital, while films under compressive strain show an enhanced occupation of the $3z^2$-r^2 orbital. These findings promote our further understanding of the subtle influence of strain on the electronic configurations of nickelates and may offer a new prospect to systematically

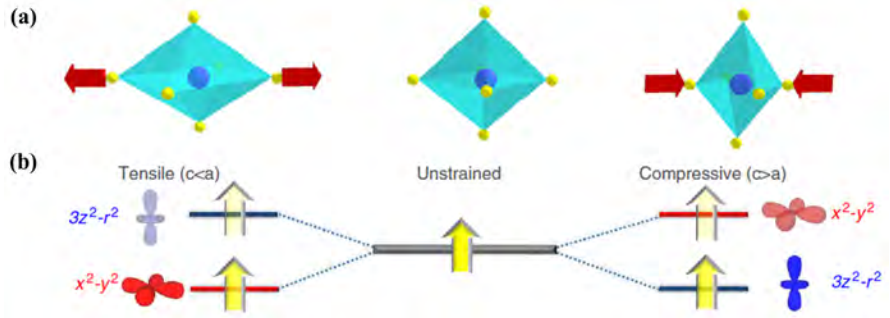

Figure 1.14: *(a) Distortion of octahedra in perovskite thin films under the three possible strain states: tensile-strain, no strain, and compressive strain. (b) The effect of strain on the e_g levels of transition metals. (Reprinted with permission from Ref. [80])*

modulate the orbital filling of perovskites by strain engineering.

1.5.4 Structural defects

When we talk about a "defect", it is equivalent to say "lack of perfection". At first sight, the defect appears to be not attractive. However, just like a coin has two sides, the existence of defects is not always bad. This is extraordinarily true in the material science. On the one hand, despite of the intensive efforts to improve the synthesis processes, defects are always present in crystals. In some cases, they indeed have a negative influence on the optical, mechanical, magnetic and electronic properties of a solid. For instance, defects in metals intensify the scattering of free electrons, leading to an increase of resistivity. However, on the other hand, the existence of defects and the modulation of their content in a solid also offers us an fantastic opportunity to tune the properties of materials. Nowadays, crystals with well-controlled defect concentrations have been commonly used in designing devices with desired functionalities. A representative example is provided by the semiconductors, in which the tunable doping of additional atoms (donors or acceptors) into the crystalline matrix, effectively modulate their electrical properties.

In a real crystal, different kinds of defects usually coexist in the lattice. According to their dimensional nature, structural defects can be roughly divided into four groups: point defects (i.e. vacancies and impurity atoms), line defects (i.e. dislocations), 2-D defects (i.e. grain boundaries or domain walls), and 3-D defects (i.e. inclusion and precipitates) [82]. Great progress had been made in the past century to characterize and understand the contributions of these structural imperfections to the material properties of different materials classes. Obviously, it is not possible within the framework of this thesis to outline the aspects of all these defect types. As

a compromise, two of them, which are usually observed in nickelate thin films, will be briefly discussed below:

Ruddlesden-Popper faults. Perovskites with ideal compositions can be described by a general formula of ABO_3, which can also be seen as a lattice of alternating $[AO]^+$ and $[BO_2]^-$ layers along the [001] direction. In the presence of excess A-cations, an additional monolayer of (001) rocksalt $[AO]^+$ can formed inside a stacking of (001) perovskite ABO_3, giving rise to a $A_{n+1}B_nO_{3n+1}$ (or, equivalently, AO-$[ABO_3]_n$) composition (see Fig. 1.15(a)). This type of structural defects are commonly reported in perovskite oxides and named as Ruddlesden-Popper (RP) faults after they were firstly found by S.N. Ruddlesden and P. Popper in 1957 [83]. In recent years, the capability to control the formation of RP faults in perovskites has become a attractive task. For example, $SrTiO_3$ containing RP faults displays tunable high-dielectric and thermoelectric properties [84, 85]. The formation of RP faults in organic–inorganic perovskites significantly promotes the photovoltaic efficiency and stability of well-designed solar cells [86, 87]. In $RENiO_3$, there also have a few studies focusing on the growth of RP faults [88–90]. Interestingly, it seems the RP faults can be very easily generated in the perovskite nickelates. Detemple *et al.* reported that two types of RP faults with different configurations (planar or 3D) were formed in $LaNiO_3/LaAlO_3$ superlattices [90]. Detailed analysis revealed that the planar RP faults are directly related to the surface steps of the substrates, while the 3D RP faults originate from the formation of local stacking faults during film growth. In addition, a study presented by Bak *et al.* unveiled the oxygen atoms in the octahedra at the RP fault plane show an obvious displacement along the out-of-plane direction and, subsequently, provide more active sites for oxygen evolution reactions [89]. However, despite of the notable structural variation, these authors found both the oxidation state of Ni^{3+} and the metallic conduction behavior of film not to be affected by the RP faults.

Oxygen vacancies. Oxygen vacancies, where the oxygen atoms are missing in some sites (see Fig. 1.15(b)), are the most well-known and well-investigated point defects in oxides. As we discussed above, oxygen vacancies prefer to be formed in the nickelate films with large tensile strain. In fact, they can be present in any kind of (strained/unstrained) oxide. This is because the synthesis of most oxides are performed in a ultra-high temperature wherein atomic diffusion is large and a frequent change of atomic positions can occur. In some cases, the oxygen atoms move from their initial positions, leaving behind empty sites and, those atoms close to the surfaces can even escape from the material leaving behind a net oxygen vacancy.

In addition to being formed during crystal growth, oxygen vacancies can also be introduced into the oxides by post treatment. The most commonly used way is the annealing of oxides under an oxygen-deficient environment, which acts as a driving force to facilitate the escape of oxygen atoms from the oxides. More interestingly, this technique enables the formation of oxygen vacancies to be achieved in a controllable

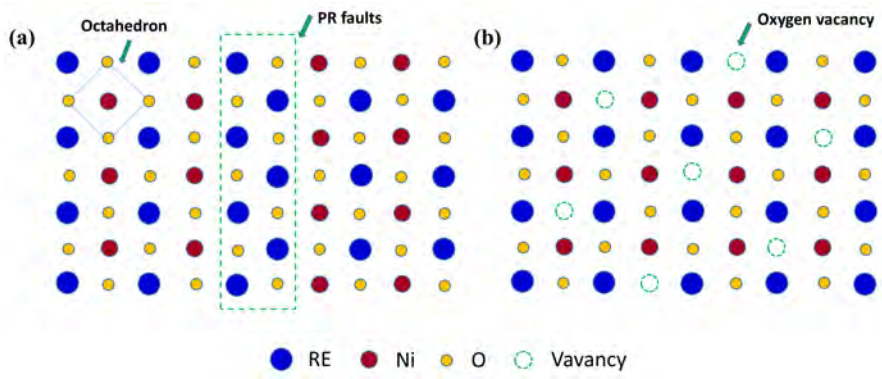

Figure 1.15: *An atomic model of (a) the RP faults and (b) the oxygen vacancies in the $RENiO_3$. The PR phase is outlined by the dashed square, the dashed circles represent the oxygen vacancies, and the rhombus indicates a octahedron in the nickelate lattice.*

way as the oxygen deficiency level in oxides is directly correlated with the annealing temperature, the annealing time, and the oxygen pressure. Control of these oxygen vacancies allows the exploitation and investigation of their contributions to properties. After decades of research, it has been realized that many properties of oxides are seriously affected, or even dominated by oxygen deficiency. Among all the properties, the modulation of electrical properties by oxygen vacancies has attracted great interest because of its possible applications in tunable electronic devices.

Physically, the contribution of oxygen vacancy to the conduction mainly arises from the 2 donated electrons left by the oxygen anion. However, the behavior of these electrons can vary substantially depending on the material. For instance, the filaments built on the oxygen vacancies generate a conducting behavior in the insulating $SrTiO_3$ as the donated electrons work as itinerant charge carriers in such kind of materials. On the contrary, the electrons localize on the adjacent octahedra in nickelates, converting the neighboring Ni cations from 3+ state to 2+ state and creating an insulating performance in this metallic oxide [91, 92]. In addition, in some oxides, the formation of oxygen vacancies is accompanied by formation of cation vacancies, producing very different overall effects [93, 94]. In addition to the generation of oxygen vacancies, their diffusion in the oxides is also of great current importance. As we will discussed later, field-driven migration of oxygen vacancies in the lattice is at the core of most memristors (resistive memory devices) and neural synaptic electronic devices based on nickelates [95, 96]. In this thesis, we have found that, for epitaxial nickelate films, the combined effect of oxygen vacancies and strain results in a very interesting evolution of the resistivity-temperature scaling [97] (see chapter 4), which allows us to come closer to understanding the mechanism for electronic transport of

this interesting class of materials (see Chapter 5).

1.5.5 Scope of applications

As a strongly correlated electron system, the $RENiO_3$, attract much attention because of their metal-insulator transition and their tunable electrical properties via pressure, strain, chemical doping and oxygen vacancies control. Whereas early works on nickelates were mainly focused on the underlying physics behind these intriguing behaviors, in recent years, the demands for exploiting their application potential becomes more and more urgent. Fortunately, interests in their applications has been triggered by several developments.

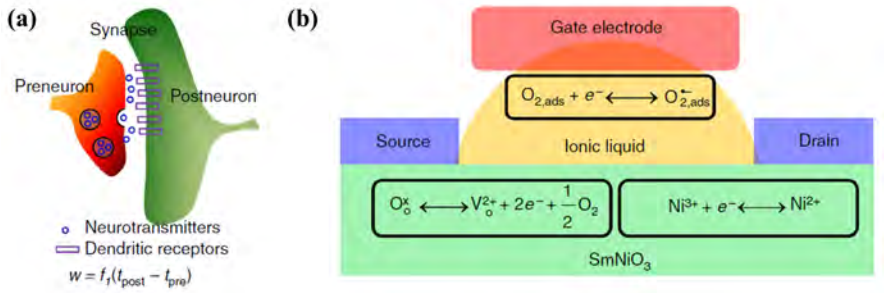

Figure 1.16: *Three-terminal nickelate synaptic transistor device. (Reprinted with permission from Ref. [95])*

Neuromorphic computing. In comparison with conventional computers, human brains have great advantages in dealing with tasks that involve processing or very large amounts of data in a faster and more power efficient way. The goal of the neuromorphic computing field is to build computers mimicking the functions of the human brain, starting form the basic elements that could partially replace transistors. To achieve a brain-like self-learning ability, the neuromorphic devices should possess a tunability similar to that required for synaptic weight in artificial neural networks (ANN), therefore allowing multiple resistance values, in contrast to the binary states allowed by transistors and current memory devices [98–101]. Interestingly, due to their tunable electrical properties, $RENiO_3$ have proved themselves as a potential candidate for this emerging application area. By employing the $SmNiO_3$ (SNO) as a channel material, a novel synaptic transistor gated by the ionic liquid was established by Shi *et al* [95]. As shown in Fig. 1.16, the source and drain in the transistor are analogues to the preneuron and postneuron terminals of a biological neuron, respectively; whilst the gated SNO channel displays a persistent and continuous change in conductivity, which emulates the evolution of synapse weight in

neurons. It is necessary to note that the conductance modulation of SNO is realized by the creation and annihilation of oxygen vacancies, as illustrated in Fig. 1.16b. Specifically, when a positive gate voltage is applied, oxygen atoms leave the SNO lattice and then the resultant oxygen vacancies convert the Ni^{3+} to Ni^{2+}. As we discussed above, the reduction of Ni valence state leads to a reduction of conductivity. Conversely, under negative voltage, this electrochemical reaction can be reversed, wherein the oxygen stored in the ionic liquid is incorporated into the SNO lattice, refilling the empty sites and recovering the conductivity correspondingly. Of course, the migration of oxygen vacancies is not the only mechanism to achieve a resistance switching in nickelates. Later on, Oh *et al.* reported that the proton doping in nickelates is also a promising way to develop a switching memory [102]. Similarly, the valence change of Ni cations is also responsible for the resistivity switching in this scenario but it is driven by the migration of protons rather than oxygen vacancies.

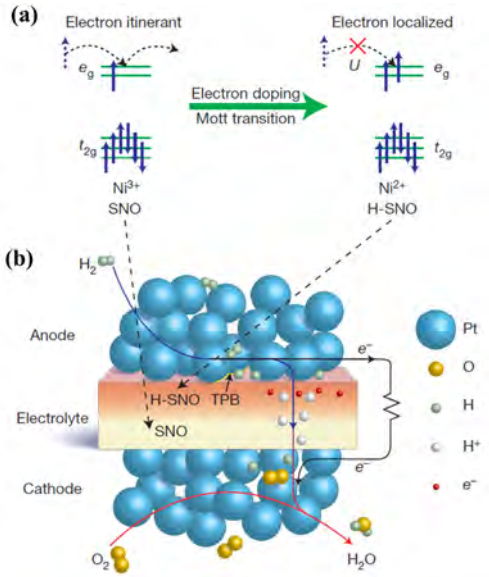

Figure 1.17: *(a) The electronic configuration of Ni 3d orbitals in initial state and localized state. (b) A schematic illustrating the operation mechanism of the SNO-electrolyte fuel cell. (Reprinted with permission from Ref. [103])*

Fuel cells. A fuel cell is a device that converts chemical energy into electrical energy by electrochemical combination of a fuel with an oxidant [104–106]. As the commonly used fuel is hydrogen, fuel cells is an environmentally-friendly way to generate electrical energy and, thus, become more attractive than traditional heat engines. In a classic design, a fuel cell consists of two electrodes: the anode and

the cathode. These two electrodes are separated by an electrolyte. When the fuel is fed to the anode, it dissociates into protons and electrons. Subsequently, the protons flow through the electrolyte under the chemical potential gradient; while, because of the screening of electrolyte, the electrons are released to the external circuit and produce direct-current electricity. Clearly, the choice of electrolyte is crucial in the whole process. To achieve a high efficiency and power output of the fuel cell, the electrolyte should not only provide an effective medium for the proton migration but should also set a strong barrier to prevent the flowing of electrons. As shown in Fig. 1.17, a recent work by Zhou *et al* demonstrated that the perovskite $RENiO_3$ with filling-controlled Mott transition is an outstanding candidate for such an electrolyte [103]. Due to their special electronic configuration, nickelates offer several advantages compared with other materials. Firstly, their extraordinary covalent bonds between Ni and O reduce the effective charge on oxygen. Correspondingly, its bonding strength with protons becomes weaker. Secondly, as the proton transfer requires local lattice distortions, the relative low energy of Ni-O bending and stretching modes in nickelates also promotes the migration of protons. Last but not least, the hydrogenation process can generate an electrically insulating layer on the surface of nickelates because of the electron doping-controlled Mott transition. In this way, the direct transport of electrons from anode to cathode is forbidden and instead they are forced to pass through the external circuit and generate electrical power. For these reasons, the fuel cell designed to employ $SmNiO_3$ as electrolyte exhibits a high-performance in energy conversation[103].

Sensors in salt water. From the discussion above, it is clear that the perovskite nickelates are good conductors for protons. Quantitatively, calculations indicate that the energy barrier associated with the proton migration in nickelates is only 0.27 eV, which is a few times smaller than other proton-conducting oxides [107]. As the incorporation of protons significantly modify the electrical properties of nickelates, it is possible to build sensors based on this mechanism. By submerging a SNO-based device into the salt water, Zhang *et al* [108] observed a robust transition from pristine state to hydrogenated state (H-SNO) under bias, accompanied with several orders of magnitude increase of resistivity. In this process, the salt water proximal to the nickelate surface dissociates into proton and OH^-, which is controlled by the value of the applied voltage. Afterwards, the protons bind to the surface oxygen firstly and then gradually intercalate into the SNO lattice. This proton influx modifies the electronic configuration of the Ni $3d$ orbitals, resulting in a notable change of conduction. Moreover, the open-circuit potential of SNO relative to the electrode is sensitive to the pH value of the solutions, such that the hydrogenation process and its resultant modification of resistivity is determined by the pH values. Combined with their inherent temperature dependence of resistivity, this SNO-based device was proposed to be an excellent sensor for detecting oceanic environments [108].

1.6 Research motivation

Strongly correlated quantum materials undergoing metal-insulator transitions (MIT) hold great promise for various applications, such as adaptable electronics, cognitive computing, photovoltaics, energy conversion, sensors, and so on. Among the materials with MIT, $RENiO_3$ present a very interesting case because their subtle structures and electronic configurations can be modified through a variety of control parameters (e.g. temperature, pressure, electron-doping, electric-field and epitaxial strain). Moreover, it has been reported that eliminating the MIT in nickelates by orbital engineering would give rise to a superconducting state, which could be more robust than that of the cuprates [109]. Thus, it becomes important to have an accurate picture of the underlying physics ruling these materials. However, despite the vast amount of recent works, transport in nickelates (as in cuprates and other electron correlated systems) is not yet fully understood. For instance, different reports postulate the nickelates either as good metals or as bad metals, as Fermi-liquid (FL), non-Fermi liquid (NFL), or even the crossover between FL and NFL. The issue of matching these different proposals in one material rises questions about the growth and the characterization of nickelate films, their defect control and the interpretation of their conduction behaviors.

In this thesis, we optimize the growth of the epitaxial nickelate films, including $NdNiO_3$, $SmNiO_3$ and $Sm_{0.6}Nd_{0.4}NiO_3$, on various single-crystalline substrates. Based on controlled post-treatment and following characterizations, we have had the chance to investigate the influence of RE radius, temperature, substrate orientation, strain, and disorder on the structural and electronic properties of nickelates. The thesis is organized as follows:

- **Chapter 2** describes the synthesis methods and characterization techniques employed in this thesis.
- **Chapter 3** introduces the modulation of the metal-insulator transition in various nickelates achieved by several parameters.
- **Chapter 4** mainly focuses on the metallic phase of the epitaxial nickelate films. We reveal a tunable resistivity-temperature scaling in $NdNiO_3$ under the combined effect of strain and disorder.
- **Chapter 5** systematically illustrates the influence of oxygen vacancies on the electrical properties of nickelates.
- **Chapter 6** provides an extended analysis of the conduction behavior of nickelates at temperatures well above room temperature.

Bibliography

[1] C. Kittel *et al.*, *Introduction to solid state physics*, vol. 8, Wiley New York, 1976.

[2] P. Drude, "Zur elektronentheorie der metalle," *Annalen der physik* **306**(3), pp. 566–613, 1900.

[3] D. R. Frear, S. N. Burchett, H. S. Morgan, and J. H. Lau, *Mechanics of solder alloy interconnects*, Springer Science & Business Media, 1994.

[4] A. Sommerfeld, "Zur elektronentheorie der metalle auf grund der fermischen statistik," *Zeitschrift für Physik* **47**(1-2), pp. 1–32, 1928.

[5] F. Bloch, "Über die quantenmechanik der elektronen in kristallgittern," *Zeitschrift für physik* **52**(7-8), pp. 555–600, 1929.

[6] W. Pauli, "Über den zusammenhang des abschlusses der elektronengruppen im atom mit der komplexstruktur der spektren," *Zeitschrift für Physik* **31**(1), pp. 765–783, 1925.

[7] P. A. M. Dirac, "On the theory of quantum mechanics," *Proceedings of the Royal Society of London. Series A, Containing Papers of a Mathematical and Physical Character* **112**(762), pp. 661–677, 1926.

[8] N. Ashcroft and N. Mermin, "Solid state physics (philadelphia, pa: Saunders college)," 1976.

[9] A. Avella, F. Mancini, *et al.*, *Strongly Correlated Systems*, Springer, 2012.

[10] E. Dagotto, "Complexity in strongly correlated electronic systems," *Science* **309**(5732), pp. 257–262, 2005.

[11] E. Morosan, D. Natelson, A. H. Nevidomskyy, and Q. Si, "Strongly correlated materials," *Advanced Materials* **24**(36), pp. 4896–4923, 2012.

[12] G. G. Natale and I. Rudnick, "Ultrasonic attenuation by conduction electrons in potassium," *Physical Review* **167**(3), p. 687, 1968.

[13] V. Gantmakher, "The experimental study of electron-phonon scattering in metals," *Reports on Progress in Physics* **37**(3), p. 317, 1974.

[14] A. Matthiessen and C. Vogt, "The electrical resistivity of alloys," *Ann. Phys. Chem.(Pogg. Folge)* **122**, pp. 19–31, 1864.

[15] M. Dressel, "Quantum criticality in organic conductors? fermi liquid versus non-fermi-liquid behaviour," *Journal of Physics: Condensed Matter* **23**(29), p. 293201, 2011.

[16] L. Landau, "Fermi fluid theory," *Zh. eksp. teor. fiz* **30**, pp. 1058–1064, 1956.

[17] L. Landau, "On the theory of the Fermi liquid," *Sov. Phys. JETP* **8**(1), p. 70, 1959.

[18] A. J. Schofield, "Non-Fermi liquids," *Contemporary Physics* **40**(2), pp. 95–115, 1999.

[19] S. Stemmer and S. J. Allen, "Non-Fermi liquids in oxide heterostructures," *Reports on Progress in Physics* **81**(6), p. 062502, 2018.

[20] S. Kasahara, T. Shibauchi, K. Hashimoto, K. Ikada, S. Tonegawa, R. Okazaki, H. Shishido, H. Ikeda, H. Takeya, K. Hirata, *et al.*, "Evolution from non-Fermi-to Fermi-liquid transport via isovalent doping in $BaFe_2(As_{1-x}P_x)_2$ superconductors," *Physical Review B* **81**(18), p. 184519, 2010.

[21] J. G. Analytis, H. Kuo, R. D. McDonald, M. Wartenbe, N. Hussey, and I. Fisher, "Transport near a quantum critical point in $BaFe_2(As_{1-x}P_x)_2$," *Nature Physics* **10**(3), pp. 194–197, 2014.

[22] D. Bonn, D. Morgan, K. Zhang, R. Liang, D. Baar, and W. Hardy, "Microwave surface impedance as a probe of unconventional superconductivity in $YBa_2Cu_3O_{6.95}$," *Journal of Physics and Chemistry of Solids* **54**(10), pp. 1297–1305, 1993.

[23] C. Pfleiderer, P. Böni, T. Keller, U. Rößler, and A. Rosch, "Non-Fermi liquid metal without quantum criticality," *Science* **316**(5833), pp. 1871–1874, 2007.

[24] H. K. Onnes, "Further experiments with liquid helium. c. on the change of electric resistance of pure metals at very low temperatures etc. iv. the resistance of pure mercury at helium temperatures," in *KNAW, Proceedings*, **13**, pp. 1910–1911, 1911.

[25] D. Li, K. Lee, B. Y. Wang, M. Osada, S. Crossley, H. R. Lee, Y. Cui, Y. Hikita, and H. Y. Hwang, "Superconductivity in an infinite-layer nickelate," *Nature* **572**(7771), pp. 624–627, 2019.

[26] O. Gunnarsson, M. Calandra, and J. Han, "Colloquium: Saturation of electrical resistivity," *Reviews of Modern Physics* **75**(4), p. 1085, 2003.

[27] N. Hussey||, K. Takenaka, and H. Takagi, "Universality of the Mott-Ioffe-Regel limit in metals," *Philosophical Magazine* **84**(27), pp. 2847–2864, 2004.

[28] S. A. Hartnoll, J. Polchinski, E. Silverstein, and D. Tong, "Towards strange metallic holography," *Journal of High Energy Physics* **2010**(4), p. 120, 2010.

[29] J. Zaanen, "Planckian dissipation, minimal viscosity and the transport in cuprate strange metals," 2019.

[30] T. Ito, K. Takenaka, and S.-i. Uchida, "Systematic deviation from T-linear behavior in the in-plane resistivity of $YBa_2Cu_3O_{7-y}$: Evidence for dominant spin scattering," *Physical review letters* **70**(25), p. 3995, 1993.

[31] A. Legros, S. Benhabib, W. Tabis, F. Laliberté, M. Dion, M. Lizaire, B. Vignolle, D. Vignolles, H. Raffy, Z. Li, *et al.*, "Universal T-linear resistivity and Planckian dissipation in overdoped cuprates," *Nature Physics* **15**(2), pp. 142–147, 2019.

[32] J. Bruin, H. Sakai, R. Perry, and A. Mackenzie, "Similarity of scattering rates in metals showing T-linear resistivity," *Science* **339**(6121), pp. 804–807, 2013.

[33] N. Doiron-Leyraud, P. Auban-Senzier, S. R. de Cotret, C. Bourbonnais, D. Jérome, K. Bechgaard, and L. Taillefer, "Correlation between linear resistivity and T_c in the Bechgaard salts and the pnictide superconductor $Ba(Fe_{1-x}Co_x)_2As_2$," *Physical Review B* **80**(21), p. 214531, 2009.

[34] H. v. Löhneysen, T. Pietrus, G. Portisch, H. Schlager, A. Schröder, M. Sieck, and T. Trappmann, "Non-Fermi-liquid behavior in a heavy-fermion alloy at a magnetic instability," *Physical review letters* **72**(20), p. 3262, 1994.

[35] Y. Cao, D. Chowdhury, D. Rodan-Legrain, O. Rubies-Bigorda, K. Watanabe, T. Taniguchi, T. Senthil, and P. Jarillo-Herrero, "Strange metal in magic-angle graphene with near Planckian dissipation," *Physical review letters* **124**(7), p. 076801, 2020.

[36] P. Cha, N. Wentzell, O. Parcollet, A. Georges, and E.-A. Kim, "Linear resistivity and Sachdev-Ye-Kitaev (SYK) spin liquid behavior in a quantum critical metal with spin-1/2 fermions," *Proceedings of the National Academy of Sciences* **117**(31), pp. 18341–18346, 2020.

[37] R. Huebener, "Conductors, semiconductors, superconductors. An introduction to solid-state physics. for physicists, engineers, and natural scientists," 2013.

[38] A. L. Éfros and B. I. Shklovskii, "Coulomb gap and low temperature conductivity of disordered systems," *Journal of Physics C: Solid State Physics* **8**(4), p. L49, 1975.

[39] B. I. Shklovskii and A. L. Efros, *Electronic properties of doped semiconductors*, vol. 45, Springer Science & Business Media, 2013.

[40] S. Kirkpatrick, "Classical transport in disordered media: scaling and effective-medium theories," *Physical Review Letters* **27**(25), p. 1722, 1971.

[41] S. Kirkpatrick, "Percolation and conduction," *Reviews of modern physics* **45**(4), p. 574, 1973.

[42] A. Miller and E. Abrahams, "Impurity conduction at low concentrations," *Physical Review* **120**(3), p. 745, 1960.

[43] N. F. Mott, "Conduction in non-crystalline materials: Iii. Localized states in a pseudogap and near extremities of conduction and valence bands," *Philosophical Magazine* **19**(160), pp. 835–852, 1969.

[44] A. Yildiz, N. Serin, T. Serin, and M. Kasap, "Crossover from nearest-neighbor hopping conduction to Efros-Shklovskii variable-range hopping conduction in hydrogenated amorphous silicon films," *Japanese Journal of Applied Physics* **48**(11R), p. 111203, 2009.

[45] R. A. Street, *Hydrogenated amorphous silicon*, Cambridge university press, 2005.

[46] J. J. van Hapert, *Hopping conduction and chemical structure: a study on silicon suboxides*. PhD thesis, 2002.

[47] S. Sharma, P. Sagar, H. Gupta, R. Kumar, and R. Mehra, "Meyer-Neldel rule in Se and S-doped hydrogenated amorphous silicon," *Solid-state electronics* **51**(8), pp. 1124–1128, 2007.

[48] M. Inada, H. Yamamoto, M. Gibo, R. Ueda, I. Umezu, S. Tanaka, T. Saitoh, and A. Sugimura, "Crossover from Efros-Shklovskii variable range hopping to nearest-neighbor hopping in silicon nanocrystal random network," *Applied Physics Express* **8**(10), p. 105001, 2015.

[49] V. Dobrosavljevic, "Introduction to metal-insulator transitions," *Conductor-Insulator Quantum Phase Transitions* , pp. 3–63, 2012.

[50] Y. Zhou and S. Ramanathan, "Mott memory and neuromorphic devices," *Proceedings of the IEEE* **103**(8), pp. 1289–1310, 2015.

[51] J. Slater, "Magnetic effects and the Hartree-Fock equation," *Physical Review* **82**(4), p. 538, 1951.

[52] N. F. Mott, "The basis of the electron theory of metals, with special reference to the transition metals," *Proceedings of the Physical Society. Section A* **62**(7), p. 416, 1949.

[53] N. Mott, "Metal-insulator transition," *Reviews of Modern Physics* **40**(4), p. 677, 1968.

[54] W. F. Brinkman and T. M. Rice, "Application of Gutzwiller's variational method to the metal-insulator transition," *Physical Review B* **2**(10), p. 4302, 1970.

[55] R. T. Scalettar, "An introduction to the Hubbard Hamiltonian," *Quantum Materials: Experiments and Theory* **6**, 2016.

[56] J. Hubbard, "Electron correlations in narrow energy bands," *Proceedings of the Royal Society of London. Series A. Mathematical and Physical Sciences* **276**(1365), pp. 238–257, 1963.

[57] S. Catalano, M. Gibert, J. Fowlie, J. Iniguez, J.-M. Triscone, and J. Kreisel, "Rare-earth nickelates $RNiO_3$: thin films and heterostructures," *Reports on Progress in Physics* **81**(4), p. 046501, 2018.

[58] J. Zaanen, G. Sawatzky, and J. Allen, "Band gaps and electronic structure of transition-metal compounds," *Physical review letters* **55**(4), p. 418, 1985.

[59] A. Bocquet, T. Mizokawa, T. Saitoh, H. Namatame, and A. Fujimori, "Electronic structure of 3d-transition-metal compounds by analysis of the 2p core-level photoemission spectra," *Physical Review B* **46**(7), p. 3771, 1992.

[60] G. Demazeau, A. Marbeuf, M. Pouchard, and P. Hagenmuller, "Sur une série de composés oxygènes du nickel trivalent derivés de la perovskite," *Journal of Solid State Chemistry* **3**(4), pp. 582–589, 1971.

[61] J. Torrance, P. Lacorre, A. Nazzal, E. Ansaldo, and C. Niedermayer, "Systematic study of insulator-metal transitions in perovskites $RNiO_3$ (R= Pr, Nd, Sm, Eu) due to closing of charge-transfer gap," *Physical Review B* **45**(14), p. 8209, 1992.

[62] R. Scherwitzl, S. Gariglio, M. Gabay, P. Zubko, M. Gibert, and J.-M. Triscone, "Metal-insulator transition in ultrathin $LaNiO_3$ films," *Physical Review Letters* **106**(24), p. 246403, 2011.

[63] J. Fowlie, "Introduction to the nickelates," in *Electronic and Structural Properties of La Ni O_3-Based Heterostructures*, pp. 19–30, Springer, 2019.

[64] J. Pérez-Cacho, J. Blasco, J. García, M. Castro, and J. Stankiewicz, "Study of the phase transitions in," *Journal of Physics: Condensed Matter* **11**(2), p. 405, 1999.

[65] J. García-Muñoz, J. Rodríguez-Carvajal, and P. Lacorre, "Neutron-diffraction study of the magnetic ordering in the insulating regime of the perovskites $RNiO_3$ (R= Pr and Nd)," *Physical Review B* **50**(2), p. 978, 1994.

[66] R. J. Green, M. W. Haverkort, and G. A. Sawatzky, "Bond disproportionation and dynamical charge fluctuations in the perovskite rare-earth nickelates," *Physical Review B* **94**(19), p. 195127, 2016.

[67] J. García-Muñoz, M. Aranda, J. Alonso, and M. Martínez-Lope, "Structure and charge order in the antiferromagnetic band-insulating phase of $NdNiO_3$," *Physical Review B* **79**(13), p. 134432, 2009.

[68] M. Medarde, C. Dallera, M. Grioni, B. Delley, F. Vernay, J. Mesot, M. Sikora, J. Alonso, and M. Martínez-Lope, "Charge disproportionation in $RNiO_3$ perovskites (R= rare earth) from high-resolution x-ray absorption spectroscopy," *Physical Review B* **80**(24), p. 245105, 2009.

[69] H. Park, A. J. Millis, and C. A. Marianetti, "Site-selective Mott transition in rare-earth-element nickelates," *Physical review letters* **109**(15), p. 156402, 2012.

[70] S. Johnston, A. Mukherjee, I. Elfimov, M. Berciu, and G. A. Sawatzky, "Charge disproportionation without charge transfer in the rare-earth-element nickelates as a possible mechanism for the metal-insulator transition," *Physical review letters* **112**(10), p. 106404, 2014.

[71] J. Varignon, M. N. Grisolia, J. Íñiguez, A. Barthélémy, and M. Bibes, "Complete phase diagram of rare-earth nickelates from first-principles," *npj Quantum Materials* **2**(1), pp. 1–9, 2017.

[72] V. Bisogni, S. Catalano, R. J. Green, M. Gibert, R. Scherwitzl, Y. Huang, V. N. Strocov, P. Zubko, S. Balandeh, J.-M. Triscone, *et al.*, "Ground-state oxygen holes and the metal-insulator transition in the negative charge-transfer rare-earth nickelates," *Nature Communications* **7**(1), pp. 1–8, 2016.

[73] T. Mizokawa, D. Khomskii, and G. Sawatzky, "Spin and charge ordering in self-doped Mott insulators," *Physical Review B* **61**(17), p. 11263, 2000.

[74] S. Middey, J. Chakhalian, P. Mahadevan, J. Freeland, A. J. Millis, and D. Sarma, "Physics of ultrathin films and heterostructures of rare-earth nickelates," *Annual Review of Materials Research* **46**, pp. 305–334, 2016.

[75] C. Bark, D. Felker, Y. Wang, Y. Zhang, H. Jang, C. Folkman, J. Park, S. Baek, H. Zhou, D. Fong, *et al.*, "Tailoring a two-dimensional electron gas at the $LaAlO_3/SrTiO_3$ (001) interface by epitaxial strain," *Proceedings of the National Academy of Sciences* **108**(12), pp. 4720–4724, 2011.

[76] J. Liu, M. Kargarian, M. Kareev, B. Gray, P. J. Ryan, A. Cruz, N. Tahir, Y.-D. Chuang, J. Guo, J. M. Rondinelli, *et al.*, "Heterointerface engineered electronic and magnetic phases of $NdNiO_3$ thin films," *Nature communications* **4**, p. 2714, 2013.

[77] E. Mikheev, A. J. Hauser, B. Himmetoglu, N. E. Moreno, A. Janotti, C. G. Van de Walle, and S. Stemmer, "Tuning bad metal and non-Fermi liquid behavior in a Mott material: Rare-earth nickelate thin films," *Science advances* **1**(10), p. e1500797, 2015.

[78] A. Malashevich and S. Ismail-Beigi, "First-principles study of oxygen-deficient $LaNiO_3$ structures," *Physical Review B* **92**(14), p. 144102, 2015.

[79] F. Conchon, A. Boulle, R. Guinebretière, E. Dooryhee, J.-L. Hodeau, C. Girardot, S. Pignard, J. Kreisel, F. Weiss, L. Libralesso, *et al.*, "Investigation of strain relaxation mechanisms and transport properties in epitaxial $SmNiO_3$ films," *Journal of Applied Physics* **103**(12), p. 123501, 2008.

[80] D. Pesquera, G. Herranz, A. Barla, E. Pellegrin, F. Bondino, E. Magnano, F. Sánchez, and J. Fontcuberta, "Surface symmetry-breaking and strain effects on orbital occupancy in transition metal perovskite epitaxial films," *Nature communications* **3**(1), pp. 1–7, 2012.

[81] M. Wu, E. Benckiser, M. Haverkort, A. Frano, Y. Lu, U. Nwankwo, S. Brück, P. Audehm, E. Goering, S. Macke, *et al.*, "Strain and composition dependence of orbital polarization in nickel oxide superlattices," *Physical Review B* **88**(12), p. 125124, 2013.

[82] W. Bollmann, *Crystal defects and crystalline interfaces*, Springer Science & Business Media, 2012.

[83] S. Ruddlesden and P. Popper, "New compounds of the K_2NiF_4 type," *Acta Crystallographica* **10**(8), pp. 538–539, 1957.

[84] S. Kamba, P. Samoukhina, F. Kadlec, J. Pokornỳ, J. Petzelt, I. Reaney, and P. Wise, "Composition dependence of the lattice vibrations in $Sr_{n+1}Ti_nO_{3n+1}$ Ruddlesden-Popper homologous series," *Journal of the European Ceramic Society* **23**(14), pp. 2639–2645, 2003.

[85] K. H. Lee, S. W. Kim, H. Ohta, and K. Koumoto, "Ruddlesden-Popper phases as thermoelectric oxides: Nb-doped SrO ($SrTiO_3$) n (n= 1, 2)," *Journal of applied physics* **100**(6), p. 063717, 2006.

[86] H. Tsai, W. Nie, J.-C. Blancon, C. C. Stoumpos, R. Asadpour, B. Harutyunyan, A. J. Neukirch, R. Verduzco, J. J. Crochet, S. Tretiak, *et al.*, "High-efficiency two-dimensional Ruddlesden-Popper perovskite solar cells," *Nature* **536**(7616), pp. 312–316, 2016.

[87] X. Zhang, R. Munir, Z. Xu, Y. Liu, H. Tsai, W. Nie, J. Li, T. Niu, D.-M. Smilgies, M. G. Kanatzidis, *et al.*, "Phase transition control for high performance Ruddlesden-Popper perovskite solar cells," *Advanced Materials* **30**(21), p. 1707166, 2018.

[88] C. Coll, L. López-Conesa, J. M. Rebled, C. Magén, F. Sanchez, J. Fontcuberta, S. Estrade, and F. Peiro, "Simulation of STEM-HAADF image contrast of Ruddlesden-Popper faulted $LaNiO_3$ thin films," *The Journal of Physical Chemistry C* **121**(17), pp. 9300–9304, 2017.

[89] J. Bak, H. B. Bae, J. Kim, J. Oh, and S.-Y. Chung, "Formation of two-dimensional homologous faults and oxygen electrocatalytic activities in a perovskite nickelate," *Nano letters* **17**(5), pp. 3126–3132, 2017.

[90] E. Detemple, Q. Ramasse, W. Sigle, G. Cristiani, H.-U. Habermeier, B. Keimer, and P. Van Aken, "Ruddlesden-popper faults in $LaNiO_3/LaAlO_3$ superlattices," *Journal of Applied Physics* **112**(1), p. 013509, 2012.

[91] M. Kotiuga, Z. Zhang, J. Li, F. Rodolakis, H. Zhou, R. Sutarto, F. He, Q. Wang, Y. Sun, Y. Wang, *et al.*, "Carrier localization in perovskite nickelates from oxygen vacancies," *Proceedings of the National Academy of Sciences* **116**(44), pp. 21992–21997, 2019.

[92] L. Wang, S. Dash, L. Chang, L. You, Y. Feng, X. He, K.-j. Jin, Y. Zhou, H. G. Ong, P. Ren, *et al.*, "Oxygen vacancy induced room-temperature metal–insulator transition in nickelate films and its potential application in photovoltaics," *ACS applied materials & interfaces* **8**(15), pp. 9769–9776, 2016.

[93] C. Lenser, A. Koehl, I. Slipukhina, H. Du, M. Patt, V. Feyer, C. M. Schneider, M. Lezaic, R. Waser, and R. Dittmann, "Formation and movement of cationic defects during forming and resistive switching in $SrTiO_3$ thin film devices," *Advanced functional materials* **25**(40), pp. 6360–6368, 2015.

[94] C. Xu, M. Moors, and R. Dittmann, "Impact of cation stoichiometry on the early stage of growth of $SrTiO_3$ deposited by pulsed laser deposition," *Applied surface science* **359**, pp. 68–72, 2015.

[95] J. Shi, S. D. Ha, Y. Zhou, F. Schoofs, and S. Ramanathan, "A correlated nickelate synaptic transistor," *Nature communications* **4**(1), pp. 1–9, 2013.

[96] S. D. Ha, J. Shi, Y. Meroz, L. Mahadevan, and S. Ramanathan, "Neuromimetic circuits with synaptic devices based on strongly correlated electron systems," *Physical Review Applied* **2**(6), p. 064003, 2014.

[97] Q. Guo, S. Farokhipoor, C. Magén, F. Rivadulla, and B. Noheda, "Tunable resistivity exponents in the metallic phase of epitaxial nickelates," *Nature Communications* **11**(1), pp. 1–9, 2020.

[98] R. Scherwitzl, P. Zubko, I. G. Lezama, S. Ono, A. F. Morpurgo, G. Catalan, and J.-M. Triscone, "Electric-field control of the metal-insulator transition in ultrathin $NdNiO_3$ films," *Advanced Materials* **22**(48), pp. 5517–5520, 2010.

[99] D. Ielmini and S. Ambrogio, "Emerging neuromorphic devices," *Nanotechnology* **31**(9), p. 092001, 2019.

[100] D. Ielmini and H.-S. P. Wong, "In-memory computing with resistive switching devices," *Nature Electronics* **1**(6), pp. 333–343, 2018.

[101] V. Milo, G. Malavena, C. Monzio Compagnoni, and D. Ielmini, "Memristive and CMOS devices for neuromorphic computing," *Materials* **13**(1), p. 166, 2020.

[102] C. Oh, S. Heo, H. M. Jang, and J. Son, "Correlated memory resistor in epitaxial $NdNiO_3$ heterostructures with asymmetrical proton concentration," *Applied Physics Letters* **108**(12), p. 122106, 2016.

[103] Y. Zhou, X. Guan, H. Zhou, K. Ramadoss, S. Adam, H. Liu, S. Lee, J. Shi, M. Tsuchiya, D. D. Fong, *et al.*, "Strongly correlated perovskite fuel cells," *Nature* **534**(7606), pp. 231–234, 2016.

[104] N. Q. Minh, "Ceramic fuel cells," *Journal of the American Ceramic Society* **76**(3), pp. 563–588, 1993.

[105] K. Saikia, B. K. Kakati, B. Boro, and A. Verma, "Current advances and applications of fuel cell technologies," in *Recent Advancements in Biofuels and Bioenergy Utilization*, pp. 303–337, Springer, 2018.

[106] L. Carrette, K. A. Friedrich, and U. Stimming, "Fuel cells: principles, types, fuels, and applications," *ChemPhysChem* **1**(4), pp. 162–193, 2000.

[107] K.-D. Kreuer, "Proton-conducting oxides," *Annual Review of Materials Research* **33**(1), pp. 333–359, 2003.

[108] Z. Zhang, D. Schwanz, B. Narayanan, M. Kotiuga, J. A. Dura, M. Cherukara, H. Zhou, J. W. Freeland, J. Li, R. Sutarto, *et al.*, "Perovskite nickelates as electric-field sensors in salt water," *Nature* **553**(7686), pp. 68–72, 2018.

[109] P. Hansmann, X. Yang, A. Toschi, G. Khaliullin, O. Andersen, and K. Held, "Turning a nickelate fermi surface into a cupratelike one through heterostructuring," *Physical review letters* **103**(1), p. 016401, 2009.